Coherent pair injection as a route towards the enhancement of supersolid order in many-body bosonic models
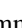
Emmanouil Grigoriou [1,*], Zhiyao Ning [2,*], Hang Su [3], Benjamin Löckler,[4] Ming Li,[1]
Yoshitomo Kamiya,[3,†] and Carlos Navarrete-Benlloch [1,4,5,6,‡]

[1]*Wilczek Quantum Center, School of Physics and Astronomy, Shanghai Jiao Tong University, Shanghai 200240, China*
[2]*Graduate School of Science and Technology, University of Tsukuba, Tsukuba 305-8571, Japan*
[3]*School of Physics and Astronomy, Shanghai Jiao Tong University, Shanghai 200240, China*
[4]*Max-Planck Institute for the Science of Light, Staudtstrasse 2, 91058 Erlangen, Germany*
[5]*Shanghai Research Center for Quantum Sciences, Shanghai 201315, China*
[6]*Departament d'Òptica i Optometria i Ciències de la Visió, Universitat de València, Dr. Moliner 50, 46100 Burjassot, Spain*

Over the past couple of decades, quantum simulators have been probing quantum many-body physics with unprecedented levels of control. So far, the main focus has been on the access to novel observables and dynamical conditions related to condensed-matter models. However, the potential of quantum simulators goes beyond the traditional scope of condensed-matter physics: Being based on driven-dissipative quantum optical platforms, quantum simulators allow for processes that typically are not considered in condensed-matter physics. These processes can enrich in unexplored ways the phase diagram of well-established models. Taking the extended Bose-Hubbard model as the guiding example, in this work we examine the impact of coherent pair injection, a process readily available in, for example, superconducting circuit arrays. The interest behind this process is that, in contrast to the standard injection of single excitations, it can be configured to preserve the U(1) symmetry underlying the model. We prove that this process favors both superfluid and density-wave order, as opposed to insulation or homogeneous states, thereby providing a route towards the access of lattice supersolidity.

I. INTRODUCTION

Macroscopic quantum states capable of surviving decoherence constitute some of the most intricate phases of matter. Understanding properties such as superconductivity and superfluidity holds the promise for key technological applications. These exotic types of behavior emerge from the interplay between different microscopic processes involving many particles and are typically associated with the phenomenon of spontaneous symmetry breaking. Recently, Feynman's idea for quantum simulation in its modern incarnation [1–7] has become of central importance. In this emerging research field, many-body complexity relies on an ever-increasing number of degrees of freedom, and in fact, extraordinary progress in recent decades has led to an explosion of experimental quantum platforms over which we

have unprecedented levels of control. It is now possible to engineer systems that can simulate quantum models expected to exhibit a rich variety of phases otherwise difficult to observe. A number of lattice models, such as the Hubbard model [8–12], are successful examples which can be experimentally implemented with, e.g., cold atoms in optical lattices [2,13,14], photonic devices [15–19], and superconducting circuits [5,20–26].

Until now, a wide range of many-body models borrowed from condensed-matter physics have been explored theoretically and experimentally in quantum simulators. In contrast, much less attention has been given to processes that do not traditionally appear in condensed-matter systems, but are available in modern simulators. Examples of these are the coherent injection of excitations or tailored dissipation [27–31]. In this work we focus on one process that stands out among this class: down-conversion, where a single excitation of a driving field is coherently transformed into two excitations of the system (and vice versa) [32–40]. In contrast to the common coherent injection of single excitations, it can be configured to preserve the symmetries that need to be spontaneously broken in order to build the macroscopic quantum coherence present in, e.g., superfluidity. Down-conversion has been a fundamental tool in quantum optics and modern technologies [41–44] and we believe that it can become a powerful tool in modern quantum simulators as well. Hence it is of paramount importance to understand emergent physics induced by this process.

---

*These authors contributed equally to the work.

†Contact author: yoshi.kamiya@sjtu.edu.cn

‡Contact author: carlos.navarrete@uv.es

As a first step towards this goal, here we address the question of which phases are favored by the presence of coherent pair injection. We focus on its action on the extended one-dimensional (1D) Bose-Hubbard model, where several types of (lattice) insulating and superfluid ground-state phases have been predicted to appear [45–49]. As a generic conclusion, we find that pair injection favors both density-wave order and superfluidity, thus effectively extending the region of the phase diagram where supersolid order is expected to appear. This opens the possibility of stabilizing supersolid phases as robust steady states once dissipation is included in the model.

II. MODEL AND MAIN RESULTS

To demonstrate the effects of pair injection on a many-body bosonic system, we consider the ground state of the extended soft-core Bose-Hubbard Hamiltonian in one dimension with the periodic boundary condition $L + 1 \rightarrow 1$,

$$
\hat{H} = \sum_{j=1}^{L} \left(-\mu \hat{n}_j + \frac{U}{2} \hat{n}_j(\hat{n}_j - 1) - \frac{\varepsilon}{2}(\hat{a}_j^{\dagger 2} + \hat{a}_j^2) \right.
$$

$$
\left. + V \hat{n}_{j+1} \hat{n}_j - J(\hat{a}_j^\dagger \hat{a}_{j+1} + \hat{a}_{j+1}^\dagger \hat{a}_j) \right), \quad (1)
$$

where the bosonic operators satisfy canonical commutation relations $[\hat{a}_j, \hat{a}_l] = 0$ and $[\hat{a}_j, \hat{a}_l^\dagger] = \delta_{jl}$. The operator $\hat{n}_j = \hat{a}_j^\dagger \hat{a}_j$ is the number operator, μ is the chemical potential, U (V) is the on-site (nearest-neighbor) repulsion energy, J is the hopping rate, and ε is the coherent pair injection rate. All parameters are taken real and positive throughout the work. This is an effective model in the sense that the full driven-dissipative problem will involve relaxation towards steady states that inherit their properties from this Hamiltonian, as we discuss at length in Sec. VII. It is also important to note that the continuous U(1) symmetry characteristic of particle-conserving Bose-Hubbard problems is replaced by a discrete Z_2 symmetry $\hat{a}_j \rightarrow -\hat{a}_j$ for $\varepsilon \neq 0$. However, in Sec. VI we extend the model to accommodate full U(1) symmetry without impacting the physics derived for the model (1), which we describe now.

When $\varepsilon = 0$, we recover the standard extended Bose-Hubbard Hamiltonian, which displays a global U(1) symmetry under $\hat{a}_j \rightarrow e^{i\theta} \hat{a}_j \; \forall \, j$ for any $\theta \in \mathbb{R}$ as well as translational symmetry $\hat{a}_j \rightarrow \hat{a}_{j+d} \; \forall \, j$ for any $d \in \mathbb{N}$. Setting aside for the moment subtleties associated with the 1D nature of the model, we review the structure of the mean-field (MF) phase diagram [45,47,50,51] in the $(zJ/U, \mu/U)$ plane (z is the lattice coordination number; $z = 2$ in our 1D case) in Fig. 1, which is convenient for introducing qualitative features of the model. The MF ground-state phases can be characterized according to which of the symmetries above are broken spontaneously. The boundary between phases with lattice superfluidity, which spontaneously break the U(1) symmetry, and insulating phases, which do not, has the well-known pancake-stack structure (which we derive analytically in Appendix B). In the presence of nearest-neighbor interactions, both of these phases can be homogeneous or staggered, leading to four types of phases: Mott insulator (MI), preserving both symmetries; density waves (DWs), breaking
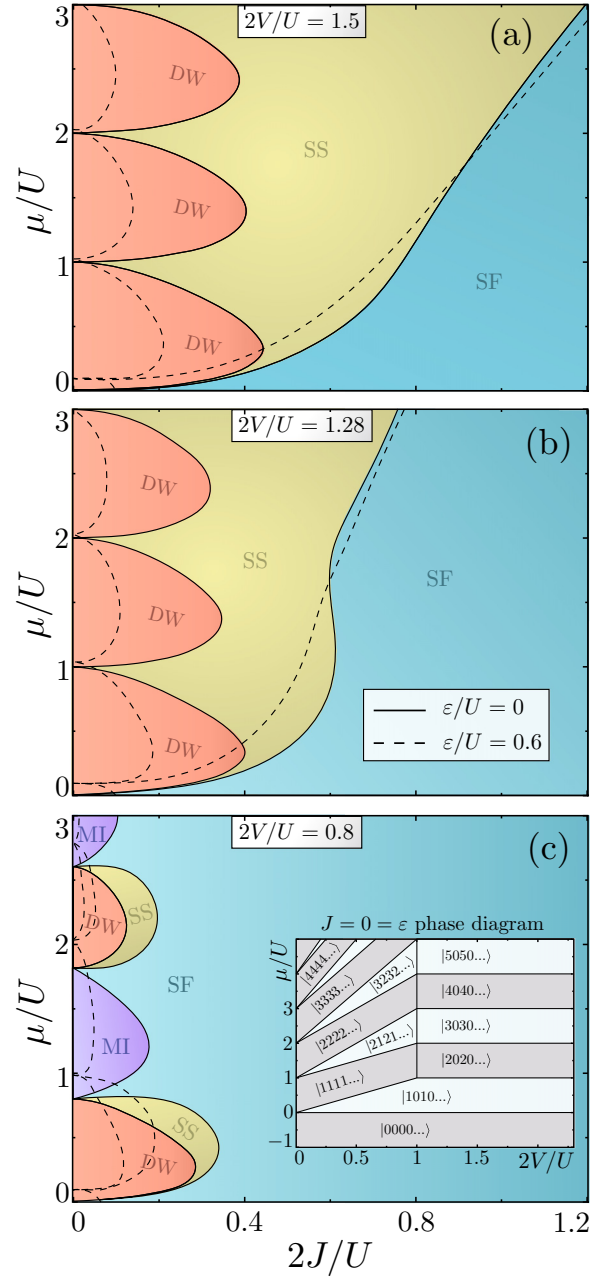
FIG. 1. MF ground-state phase diagram in the $(2J/U, \mu/U)$ plane for representative values of $2V/U$. Here DW and MI (SF and SS) refer to density-wave and Mott insulating (homogeneous-superfluid and supersolid) phases, respectively. The solid lines correspond to $\varepsilon = 0$ while the dashed lines represent how the boundaries move as ε increases. The phase boundaries have been artificially smoothened out for clarity (see the raw data in Appendix B). The inset in (c) shows the $J = 0 = \varepsilon$ phase diagram in the $(\mu/U, 2V/U)$ plane, with Fock states $|n_1 n_2 n_3 n_4 \cdots \rangle$.

translational symmetry only; superfluid (SF), breaking only U(1); and supersolid (SS), breaking both symmetries. For $0 < 2V/U < 1$ the insulating domes alternate between MI and DW phases, with SS phases appearing as a small region over DW domes. In contrast, for $2V/U > 1$ MI phases disappear, and SS phases are able to take over a larger portion of

the superfluid region, generating a SS-SF boundary that tends to a straight line for large densities.

We identify ground-state phases by analyzing the correlation functions

$$C_{\text{SF}}(j, l) = \langle \hat{a}_j^\dagger \hat{a}_l \rangle, \tag{2a}$$

$$C_{\text{DW}}(j, l) = \langle \delta\hat{n}_j \delta\hat{n}_l \rangle, \tag{2b}$$

with density fluctuations $\delta\hat{n}_j = \hat{n}_j - \sum_{j=1}^{L}\langle \hat{n}_j \rangle/L$ [47]. In the insulating phases, $C_{\text{SF}}(j, l)$ decays exponentially (or faster) with the distance $|j - l|$; in contrast, it remains finite or decays as a power law in superfluid phases. Moreover, spatially ordered phases such as DW or SS present subexponential decay of $C_{\text{DW}}(j, l)$.

In the presence of pair injection ($\varepsilon \neq 0$), the rigorous presence of superfluid order is ruled out, but it still allows for spontaneous Z_2 symmetry breaking associated with the θ-phase order. Whenever a remark on the discreteness of the phase is needed, we denote its corresponding phases by Z_2SF and Z_2SS. Nevertheless, as we mentioned above, we show in Sec. VI that the model (1) can be extended to restore a full U(1) symmetry without impacting our main conclusions.

In the following we analyze the ground states of (1) using complementary approaches: the density-matrix renormalization group (DMRG), a powerful variational optimization algorithm for low-dimensional systems, to demonstrate our main point conclusively; MF approximation for a more exhaustive check of the parameter space; the coherent-state ansatz to obtain analytical insight; and finally the Gaussian-state ansatz to confirm the robustness of the coherent-state ansatz predictions. All these methods converge to two basic conclusions. First, pair injection ε generally favors the Z_2 superfluid phases over the insulating ones; in other words, the insulating regions of the phase diagram shrink as we increase ε. Second, more intriguingly, deep in the region with broken phase symmetry, ε favors Z_2SS order over Z_2SF order. While this is a subtle trend in Fig. 1 that focuses on the small-J/U region, it becomes more and more evident as one gets deeper into the superfluid (large-J/U) region (note that the Z_2SS-Z_2SF boundary lines for $\varepsilon = 0$ and $\varepsilon \neq 0$ cross as J/U increases, such that for larger J/U the critical μ/U separating them is smaller for $\varepsilon \neq 0$). We discuss these results at length throughout the following sections.

III. DMRG RESULTS

We run DMRG using a matrix-product-state ansatz [52–54]. To simulate the soft-core bosonic model we introduce a truncation in the maximum occupation number per site, N_L. The accuracy of the ansatz is controlled by the bond dimension χ, which determines the degree of many-body entanglement available in the ansatz. In the results presented below, we have checked convergence of the correlation functions (2), as well as the energy and the bipartite entanglement entropy, requiring $N_L = 10$ and $\chi = 4000$ in the hardest cases.

To determine the ground state for a given parameter set, we perform a finite-size scaling of the correlation ratios [55]

$$R_{\text{SF}} = \frac{C_{\text{SF}}(L/2)}{C_{\text{SF}}(L/4)}, \quad R_{\text{DW}} = \frac{C_{\text{DW}}(L/2)}{C_{\text{DW}}(L/4)}, \tag{3}$$

where $C_{\text{SF/DW}}(d) \equiv C_{\text{SF/DW}}(j, j + d)$ and the ratios are independent of j. These ratios are expected to approach 1 as $L \rightarrow \infty$ when the system has long-range order or fall to 0 if the corresponding correlation function decays exponentially. We also use the Binder cumulant [56]

$$B_{\text{DW}} = \frac{1}{2}\left(3 - \frac{\langle \hat{\phi}^4 \rangle}{\langle \hat{\phi}^2 \rangle^2}\right), \tag{4}$$

which is defined to behave as $B_{\text{DW}} \rightarrow 1$ ($B_{\text{DW}} \rightarrow 0$) for $L \rightarrow \infty$ in the phase with (without) density-wave order. Here $\hat{\phi} = \sum_{l=1}^{L/2}(\hat{n}_{2l-1} - \hat{n}_{2l})$ is the density-wave order parameter. The B_{DW} turns out to be less sensitive to finite-size effects in our model and thus better suited for analyzing a density-wave transition. In addition, B_{DW}, as well as R_{SF} and R_{DW}, is expected to be system-size independent at a critical point and therefore form a crossing point between curves with different L.

In Fig. 2(a) we first examine the impact of the injection rate ε on the phase boundary between the insulating and Z_2 superfluid regions. We set $2V/U = 1.5$ and $\mu/U = 1.8$ and show R_{SF} as a function of $2J/U$ for different values of ε/U. The observed tendency towards a step function for larger L suggests a second-order transition. We also observe that the superfluid phase is enlarged as ε increases (the crossing occurs for lower $2J/U$). The same conclusion is drawn for any other set of parameters we have tested with DMRG.

In Figs. 2(b) and 2(c) we analyze the Z_2SF-Z_2SS boundary. We set $2V/U = 1.5$ and $2J/U = 0.8$, for which we confirm $R_{\text{SF}} \rightarrow 1$ as $L \rightarrow \infty$ irrespective of the remaining parameters, meaning that the ground state retains the Z_2 superfluid order in the entire (μ/U, ε/U) plane shown here. Figure 2(b) shows R_{DW} in the (μ/U, ε/U) parameter space for $L = 16$, together with the critical points (thick solid line) that we determine by performing a finite-size scaling analysis of B_{DW}, as shown in Fig. 2(c). Except for very low densities (small $2J/U$ and ε/U), it is clear that the boundary separating the Z_2SF ($R_{\text{DW}} \rightarrow 0$) and the Z_2SS ($R_{\text{DW}} \rightarrow 1$) regions moves down as ε increases, concluding that pair injection extends the supersolid region. Moreover, for larger ε there is a clear linear tendency of the boundary on ε. Indeed, our coherent-state ansatz (see Sec. V) predicts a critical μ given by

$$\mu_c = 4J(2V/U - 1)^{-1} - \varepsilon \tag{5}$$

and existing for $2V/U > 1$. Note that Eq. (5) also predicts a linear relation between μ_c and $2J$ with slope $2/(2V/U - 1)$, which is consistent with previous $\varepsilon = 0$ numerical results [48] and with the MF picture described above. Hence, our high-precision DMRG calculation allows us to univocally conclude that pair injection favors Z_2SS.

IV. MF APPROACH

To show that the enhancement of supersolidity via pair injection can be expected for a wider parameter range, we extend the well-known [50,57–59] MF approach by incorporating the ε term. The MF approximation is based on a separable ansatz of the type $\bigotimes_{j=1}^{L} |\psi_j\rangle$, which ensures that the

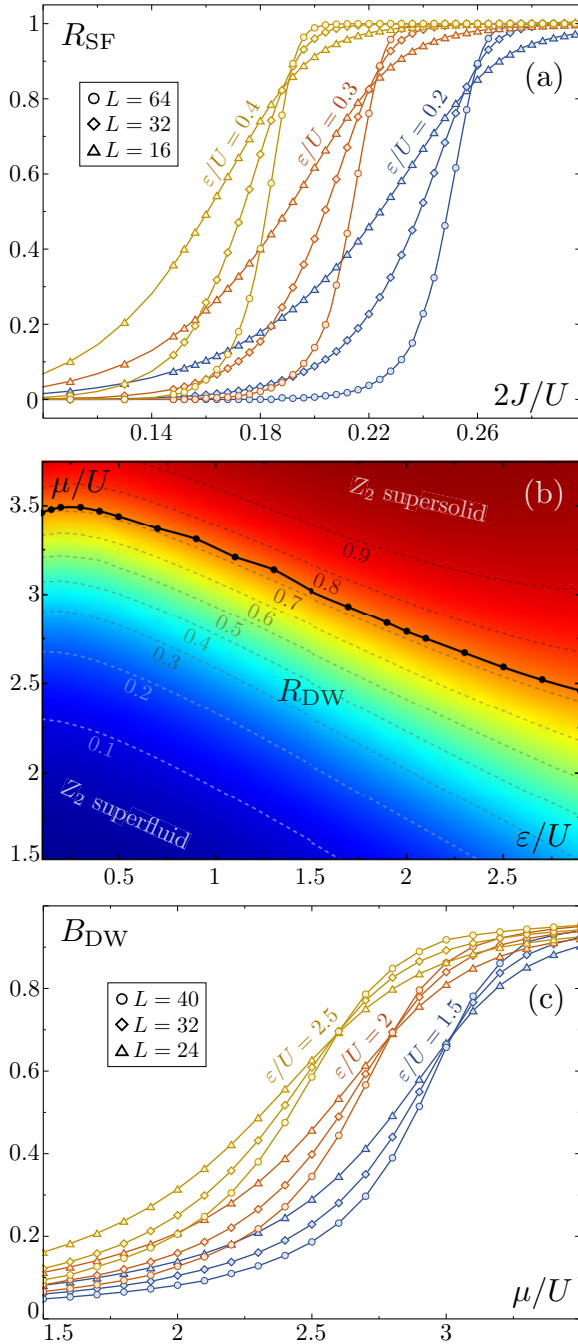FIG. 2. (a) R_{SF} as a function of $2J/U$ for different values of L and ε/U with $\mu/U = 1.8$ and $2V/U = 1.5$. As ε/U increases, a smaller value of $2J/U$ can bring the system to a quantum critical point separating insulating and Z_2 superfluid phases. (b) R_{DW} in the $(\mu/U, \varepsilon/U)$ plane with $2J/U = 0.8$ for $L = 16$. The Z_2 phase symmetry is broken in the entire region shown here. (c) Binder parameter B_{DW} as a function of μ/U for different values of L and ε/U with $2J/U = 0.8$. The crossing points determine the critical μ/U for each ε/U and are shown in (b) as black dots. (b) and (c) show that ε clearly favors density-wave order in the superfluid region, that is, supersolidity.

coupling between the quantum fluctuations at different lattice sites is negligible. In particular, given two operators $\hat{A}$ and $\hat{B}$ acting on different sites, and their corresponding fluctuations

$\delta\hat{A} = \hat{A} - \langle\hat{A}\rangle$ and $\delta\hat{B} = \hat{B} - \langle\hat{B}\rangle$, we have

$$\hat{A}\hat{B} = (\langle\hat{A}\rangle + \delta\hat{A})(\langle\hat{B}\rangle + \delta\hat{B}) \approx \langle\hat{A}\rangle\langle\hat{B}\rangle + \langle\hat{A}\rangle\delta\hat{B} + \langle\hat{B}\rangle\delta\hat{A}$$

$$= \langle\hat{A}\rangle\hat{B} + \langle\hat{B}\rangle\hat{A} - \langle\hat{A}\rangle\langle\hat{B}\rangle. \qquad (6)$$

In our Hamiltonian (1) we find two of such type of terms, the hopping and the nearest-neighbors interaction, which we rewrite under the MF approximation as

$$\hat{a}_j^\dagger \hat{a}_{j+1} \approx \phi_j^* \hat{a}_{j+1} + \hat{a}_j^\dagger \phi_{j+1} - \phi_j^* \phi_{j+1}, \quad \text{with} \quad \phi_j = \langle\hat{a}_j\rangle, \qquad (7a)$$

$$\hat{n}_j \hat{n}_{j+1} \approx \rho_j \hat{n}_{j+1} + \hat{n}_j \rho_{j+1} - \rho_j \rho_{j+1}, \quad \text{with} \quad \rho_j = \langle\hat{n}_j\rangle. \qquad (7b)$$

The Hamiltonian then takes the form

$$\hat{H} \approx \sum_{j=1}^{L} \hat{h}_j + \mathcal{E} \equiv \hat{H}_{\mathrm{MF}}, \qquad (8)$$

with local Hamiltonian operators

$$\hat{h}_j = -[\mu - V(\rho_{j-1} + \rho_{j+1})]\hat{n}_j - \frac{\varepsilon}{2}(\hat{a}_j^2 + \hat{a}_j^{\dagger 2})$$

$$+ \frac{U}{2}\hat{n}_j(\hat{n}_j - 1) - J[(\phi_{j-1}^* + \phi_{j+1}^*)\hat{a}_j + \text{H.c.}] \qquad (9)$$

and a constant term

$$\mathcal{E} = \sum_{j=1}^{L}[J(\phi_j^* \phi_{j+1} + \phi_j \phi_{j+1}^*) - V\rho_j \rho_{j+1}]. \qquad (10)$$

The mean-field Hamiltonian $\hat{H}_{\mathrm{MF}}$ is a collection of local Hamiltonians coupled through the $\{\phi_j, \rho_j\}_{j=1,2,\dots,L}$ expectation values. Hence, finding the ground state becomes a nonlinear problem, since the $\hat{h}_j$'s depend on the state one is trying to determine. The problem is simplified even further by noting that we expect the ground state to be invariant under translations by an even number of sites. Denoting by $j = \mathrm{e}$ and $j = \mathrm{o}$ some reference odd and even sites, respectively, so that the ansatz can be rewritten as $\bigotimes_{j=1}^{L/2} |\psi_\mathrm{o}\rangle \otimes |\psi_\mathrm{e}\rangle$, finding the MF ground state becomes then equivalent to finding the common ground states $|\psi_\mathrm{o}\rangle$ and $|\psi_\mathrm{e}\rangle$ of the local operators

$$\hat{h}_\mathrm{o}(|\psi_\mathrm{e}\rangle) = -(\mu - 2V\rho_\mathrm{e})\hat{n}_\mathrm{o} - \frac{\varepsilon}{2}(\hat{a}_\mathrm{o}^2 + \hat{a}_\mathrm{o}^{\dagger 2})$$

$$+ \frac{U}{2}\hat{n}_\mathrm{o}(\hat{n}_\mathrm{o} - 1) - 2J(\phi_\mathrm{e}^* \hat{a}_\mathrm{o} + \phi_\mathrm{e}\hat{a}_\mathrm{o}^\dagger), \quad (11a)$$

$$\hat{h}_\mathrm{e}(|\psi_\mathrm{o}\rangle) = -(\mu - 2V\rho_\mathrm{o})\hat{n}_\mathrm{e} - \frac{\varepsilon}{2}(\hat{a}_\mathrm{e}^2 + \hat{a}_\mathrm{e}^{\dagger 2})$$

$$+ \frac{U}{2}\hat{n}_\mathrm{e}(\hat{n}_\mathrm{e} - 1) - 2J(\phi_\mathrm{o}^* \hat{a}_\mathrm{e} + \phi_\mathrm{o}\hat{a}_\mathrm{e}^\dagger), \quad (11b)$$

respectively. The notation emphasizes that $\hat{h}_\mathrm{o}$ and $\hat{h}_\mathrm{e}$ depend on the state of the even and odd sites $|\psi_\mathrm{e}\rangle$ and $|\psi_\mathrm{o}\rangle$, respectively. Starting from an initial guess for these states, or rather the expectation values $\{\phi_j, \rho_j\}_{j=\mathrm{o},\mathrm{e}}$, we find the ground state of $\hat{h}_\mathrm{o}(|\psi_\mathrm{e}\rangle)$ and $\hat{h}_\mathrm{e}(|\psi_\mathrm{o}\rangle)$, update the states $|\psi_\mathrm{o}\rangle$ and $|\psi_\mathrm{e}\rangle$, and iterate the procedure as many times as required for $\langle\hat{H}\rangle$ to converge. This is sometimes called a self-consistent Hartree-Fock procedure. We perform the calculation in the
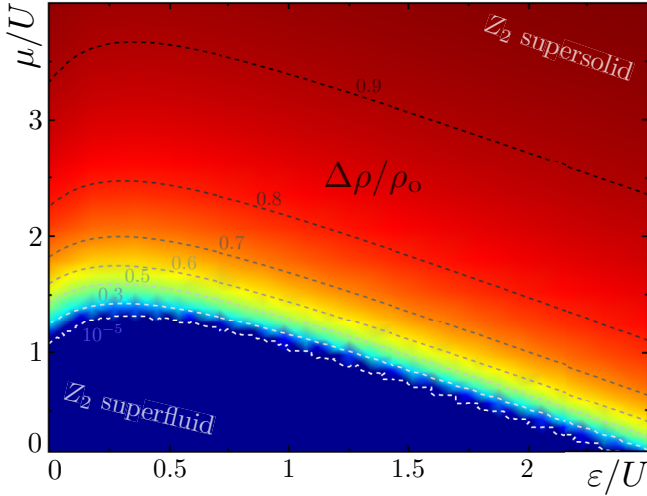
FIG. 3. MF results for the DW order parameter $\Delta\rho/\rho_\text{o} = (\rho_\text{o} - \rho_\text{e})/\rho_\text{o}$ (odd-even relative density difference) for $2J/U = 0.8$ and $2V/U = 1.5$, illustrating that pair injection in the case of a relatively small hopping rate favors $Z_2\text{SS}$ over the homogeneous $Z_2\text{SF}$, except for the perturbative region (small ε). We assume $\rho_\text{o} \geqslant \rho_\text{e}$ for definiteness.

local (truncated) Fock basis $\{|n\rangle\}_{n=0,1,\ldots,N}$, with $\hat{n}_j|n\rangle = n|n\rangle$, where N is a suitable truncation ($N = 20$ is usually enough to reach high accuracy in the parameter region analyzed in this work). For a given parameter set, we perform the self-consistent Hartree-Fock procedure starting from several educated or random guesses $\{\phi_j, \rho_j\}_{j=\text{o,e}}$ and then choose among all final states the one leading to the smallest $\langle\hat{H}\rangle$. The phase of the system is then characterized by the following conditions ($\Delta\rho = \rho_\text{o} - \rho_\text{e}$):

$$
\begin{aligned}
\phi_\text{o} = 0 = \phi_\text{e}, \quad &\Delta\rho = 0 \quad \text{(Mott insulator)}, \\
\phi_\text{o} = 0 = \phi_\text{o}, \quad &\Delta\rho \neq 0 \quad \text{(density-wave insulator)}, \\
\phi_\text{o} = \phi_\text{e} \neq 0, \quad &\Delta\rho = 0 \quad \text{(homogeneous Z_2 superfluid)}, \\
\phi_\text{o} \neq \phi_\text{e}, \quad &\Delta\rho \neq 0 \quad \text{(Z_2 supersolid)}.
\end{aligned}
\tag{12}
$$

The results shown in Figs. 1 and 3 support the conclusions drawn with DMRG. The $(2J/U, \mu/U)$ phase diagram of Fig. 1 illustrates how the insulating lobes shrink as ε increases. Moreover, for $2V/U > 1$ the $Z_2\text{SF}$-$Z_2\text{SS}$ phase boundary for large $2J/U$ asymptotically follows the coherent-state prediction (5), demonstrating that the supersolid phase is enlarged with ε. This linear tendency is most clearly observed in Fig. 3, where we set $2J/U = 0.8$ (for which $\phi_j \neq 0$) and represent $\Delta\rho/\rho_\text{o}$ in the $(\varepsilon/U, \mu/U)$ plane (for definiteness we assume $\rho_\text{o} \geqslant \rho_\text{e}$). The critical boundary separating $\Delta\rho = 0$ ($Z_2\text{SF}$) from $\Delta\rho \neq 0$ ($Z_2\text{SS}$) has a positive slope for small ε/U, but very early the slope changes sign, quickly adhering to the expected linear relation of Eq. (5), similarly to the DMRG results of Fig. 2(b). We remark that the region with initial positive slope shrinks as $2J/U$ increases.

Let us point out that the boundaries of the phase diagrams of Fig. 1 have been smoothened for ease of presentation. For completeness, in Appendix B we provide the same diagrams plotted from the raw data without any smoothing.

V. COHERENT-STATE ANSATZ

We introduce now another variational treatment that allows us to obtain an analytical estimation of the $Z_2\text{SF}$-$Z_2\text{SS}$ boundary. We use a coherent-state ansatz [35,36,44] $\bigotimes_{j=1}^{L} |\alpha_j\rangle$, with $\hat{a}_j|\alpha_j\rangle = \alpha_j|\alpha_j\rangle$ and $\{\alpha_j \in \mathbb{C}\}_{j=1,2,\ldots,L}$. For large $2J/U$, the ground state can be expected to develop a large superfluid order parameter ϕ_j and therefore to be dominated by a strong coherent component α_j. Indeed, we find that the overlap between the MF state and the coherent-state ansatz is above 90% at all investigated points, increasing with $2J/U$ and ε/U.

In the coherent-state ansatz, the uniform superfluid and supersolid phases are distinguished by whether the coherent amplitude is uniform ($\alpha_j = \alpha \,\forall\, j$) or staggered ($|\alpha_j| \neq |\alpha_{j+1}|$ and $\alpha_j = \alpha_{j+2}$). In the following we determine analytically these type of solutions and show how they lead to the formula (5) for the $Z_2\text{SF}$-$Z_2\text{SS}$ boundary. The variational energy functional $\langle\hat{H}\rangle$ assumes the following polynomial form as a function of the coherent amplitudes α_j:

$$
\begin{aligned}
E = \sum_{j=1}^{L} \bigg(&-\mu|\alpha_j|^2 - J(\alpha_j\alpha_{j+1}^* + \alpha_j^*\alpha_{j+1}) \\
&- \frac{\varepsilon}{2}(\alpha_j^2 + \alpha_j^{*2}) + \frac{U}{2}|\alpha_j|^4 + V|\alpha_j|^2|\alpha_{j+1}|^2 \bigg).
\end{aligned}
\tag{13}
$$

The J term is minimized when all sites have the same phase so that $\text{Re}(\alpha_j\alpha_{j+1}^*) \geqslant 0$. On the other hand, in order to minimize the ε term, the amplitudes α_j must be real. Hence, we conclude that the amplitudes are real and either all positive or all negative. In contrast, since the energy functional is invariant under the Z_2 transformation $\alpha_j \to -\alpha_j \,\forall\, j$, we can take the positive sign for the amplitudes for definiteness, just keeping in mind that from any minimizing configuration $\{\alpha_j \geqslant 0\}_{j=1,2,\ldots,L}$ we can build an equally valid configuration simply by inverting the sign of all amplitudes. The minimization condition $\partial E/\partial\alpha_j = 0$ becomes then

$$
\big[-(\mu+\varepsilon) + U\alpha_j^2 + V\alpha_{j+1}^2 + V\alpha_{j-1}^2\big]\alpha_j = J(\alpha_{j+1} + \alpha_{j-1}),
\tag{14}
$$

with α_j real and positive for all j. These equations possess three types of analytic solutions, which happen to be the only relevant minima according to our exhaustive numerical exploration, as we discuss in Appendix C. The simplest among these is the trivial one, $\alpha_j = 0 \,\forall\, j$, with null energy $E = 0$ in all parameter space. One can also easily find in (14) a nontrivial homogeneous solution (which we simply denote by Z_2 superfluid or SF in this coherent context)

$$
\alpha_j = \sqrt{\frac{\mu + \varepsilon + 2J}{U + 2V}} \equiv \alpha_\text{SF} \,\forall\, j,
\tag{15}
$$

with energy

$$
E = -2LJ^2 \frac{(\nu+1)^2}{U+2V} \equiv E_\text{SF} < 0,
\tag{16}
$$

where we have defined the parameter $\nu = (\mu+\varepsilon)/2J$ that will reappear throughout this section on occasion. This SF solution has then lower energy than the trivial one. If we

would allow for negative chemical potentials, this superfluid solution would cease to exist as soon as $\mu < -(\varepsilon + 2J)$ or $\nu < -1$, the parameter region where the trivial solution takes over (actually, for $\nu < -1$ the trivial solution is a minimum, while for $\nu > -1$ it becomes an unstable saddle point). However, this is not relevant to our present work where we are analyzing the $\mu > 0$ region, since this is the usual accessible region in condensed-matter physics.

The third analytic solution is the staggered one (which we denote by Z_2 supersolid or SS)

$$\alpha_j = \begin{cases} \alpha_{\mathrm{SS}} & \text{for } j \in \text{odd} \\ r\alpha_{\mathrm{SS}} & \text{for } j \in \text{even,} \end{cases} \tag{17}$$

where we assume that the density is larger at odd sites ($0 \leqslant r \leqslant 1$) for definiteness, but the opposite case is also a solution, owed to the translational invariance of the Hamiltonian. Particularizing (14) to odd j leads to

$$\alpha_{\mathrm{SS}}^2 = \frac{\mu + \varepsilon + 2rJ}{U + 2r^2V}, \tag{18}$$

which inserted into (14) particularized now to even j leads to an equation for r that reads

$$(1 - r^2)(1 + r^2 - ar) = 0, \tag{19}$$

where we have defined $a = \nu(2V/U - 1)$. Apart from the $r = 1$ root that simply leads to the SF solution discussed above, we obtain another root satisfying $0 \leqslant r \leqslant 1$, namely, $2r = a - \sqrt{a^2 - 4}$, which exists only for $a \geqslant 2$, a condition that can be recast as

$$\frac{V}{U} \geqslant \frac{1}{2} + \frac{1}{\nu} \Leftrightarrow \mu \geqslant \frac{4J}{2V/U - 1} - \varepsilon. \tag{20}$$

Let us remark that the equality in this expression leads precisely to the SF-SS boundary that we have presented in (5). Indeed, for $a = 2$ we get $r = 1$, meaning that the staggered solution converges to the homogeneous one at the boundary. Moreover, inserting the staggered solution into the coherent energy functional (13) leads to

$$E = -\frac{LJ^2}{U}\left(\nu^2 + \frac{2}{2V/U - 1}\right) \equiv E_{\mathrm{SS}}, \tag{21}$$

which is easily shown to be smaller than E_{SF} in all the domain of existence of the solution. Hence, we conclude that $a = 2$ is the coherent-state prediction for the phase boundary between the SF and SS regions. This method predicts a continuous second-order phase transition, since E_{SF} and E_{SS} and their first-order derivatives are continuously connected at the phase boundaries, with the discontinuity appearing at the second-order derivative. The coherent-state ansatz provides then a phase diagram that is easily summarized in terms of just two relevant parameters ν and $2V/U$, as we show in Fig. 4. Let us remark that these results are confirmed also when considering a fully general Gaussian ansatz, which we present in Appendix D.

VI. MODEL WITH FULL U(1) SYMMETRY

The pair-injection term $-\sum_j \varepsilon(\hat{a}_j^2 + \hat{a}_j^{\dagger 2})/2$ considered in previous sections explicitly breaks the U(1) symmetry of the
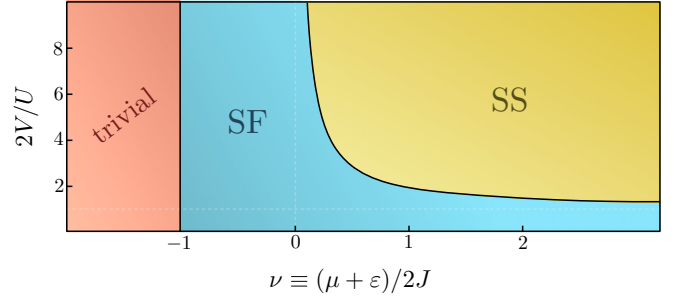

FIG. 4. Phase diagram arising from the coherent-state ansatz, which is fully characterized by two reduced parameters only, $\nu = (\mu + \varepsilon)/2J$ and V/U. The trivial phase refers to the $\alpha_j = 0$ configuration for all coherent amplitudes (vacuum state). Here SF refers to a configuration with all amplitudes equal and nonzero (homogeneous superfluidlike) and SS refers to a configuration with alternating amplitudes, different for even and odd sites (supersolidlike). The boundary between the trivial and SF phases is $\nu = -1$. The boundary between SF and SS phases is $2V/U = 1 + 2/\nu$ and exists only for $\nu > 0$ and $2V/U > 1$.

extended Bose-Hubbard model, leaving only a Z_2 symmetry $\hat{a}_j \rightarrow -\hat{a}_j \, \forall \, j$. However, as we mentioned in the Introduction, one can consider more elaborate extensions of the Bose-Hubbard model with pair-injection terms that still possess full U(1) symmetry. Here we put forward one such model and show that, at the coherent-state-ansatz level, pair injection has the same effect as in the simpler model (1) studied in the previous sections.

Consider a chain with two bosonic modes per site, with annihilation operators $\{\hat{a}_j, \hat{b}_j\}_{j=1,2,\dots,L}$, satisfying canonical commutation relations $[\hat{a}_j, \hat{a}_l^\dagger] = \delta_{jl} = [\hat{b}_j, \hat{b}_l^\dagger]$ with any other commutator vanishing. Each set of bosonic modes is subject to an extended Bose-Hubbard Hamiltonian

$$\hat{H}_a = \sum_{j=1}^{L} \left(-\mu\hat{a}_j^\dagger\hat{a}_j + \frac{U}{2}\hat{a}_j^{\dagger 2}\hat{a}_j^2 \right.$$
$$\left. -J(\hat{a}_j^\dagger\hat{a}_{j+1} + \hat{a}_{j+1}^\dagger\hat{a}_j) + V\hat{a}_{j+1}^\dagger\hat{a}_{j+1}\hat{a}_j^\dagger\hat{a}_j \right), \tag{22a}$$

$$\hat{H}_b = \sum_{j=1}^{L} \left(-\mu\hat{b}_j^\dagger\hat{b}_j + \frac{U}{2}\hat{b}_j^{\dagger 2}\hat{b}_j^2 \right.$$
$$\left. -J(\hat{b}_j^\dagger\hat{b}_{j+1} + \hat{b}_{j+1}^\dagger\hat{b}_j) + V\hat{b}_{j+1}^\dagger\hat{b}_{j+1}\hat{b}_j^\dagger\hat{b}_j \right), \tag{22b}$$

with the different modes coupled locally through the particle nonconserving term

$$\hat{H}_{ab} = -\sum_{j=1}^{L} \varepsilon(\hat{a}_j\hat{b}_j + \hat{a}_j^\dagger\hat{b}_j^\dagger). \tag{23}$$

Just as in the previous model, this term injects pairs of excitations in the system, but now the excitations are distinguishable (nondegenerate pair injection). The resulting Hamiltonian $\hat{H} = \hat{H}_a + \hat{H}_b + \hat{H}_{ab}$ is invariant under continuous

transformations of the relative phase between the modes, that is, $\{\hat{a}_j \to e^{i\theta}\hat{a}_j, \hat{b}_j \to e^{-i\theta}\hat{b}_j\} \forall j$ and $\theta \in \mathbb{R}$, providing a U(1) symmetry to the model.

We consider now a coherent-state ansatz of the form $\bigotimes_{j=1}^L |\alpha_j, \beta_j\rangle$, with $\hat{a}_j|\alpha_j, \beta_j\rangle = \alpha_j|\alpha_j, \beta_j\rangle$ and $\hat{b}_j|\alpha_j, \beta_j\rangle = \beta_j|\alpha_j, \beta_j\rangle$, where $\{\alpha_j \in \mathbb{C}, \beta_j \in \mathbb{C}\}_{j=1,2,\ldots,L}$ are the variational parameters. The energy functional $\langle \hat{H} \rangle$ takes the form

$$E = \sum_{j=1}^L \left(-\mu(|\alpha_j|^2 + |\beta_j|^2) - 2J \operatorname{Re}(\alpha_j\alpha_{j+1}^* + \beta_j\beta_{j+1}^*) \right.$$
$$- 2\varepsilon \operatorname{Re}(\alpha_j\beta_j) + \frac{U}{2}(|\alpha_j|^4 + |\beta_j|^4)$$
$$\left. + V(|\alpha_j|^2|\alpha_{j+1}|^2 + |\beta_j|^2|\beta_{j+1}|^2) \right). \tag{24}$$

As in our original model (1), the J term is minimized when the complex amplitudes of all sites have the same phase. In addition, the ε term is minimized when each product $\alpha_j\beta_j$ is real and positive, that is, the phase sum of α_j and β_j is an integer multiple of 2π. Of course, the symmetry of the model allows the relative phase between α_j and β_j to be arbitrary, that is, given a minimizing configuration $\{\alpha_j, \beta_j\}_{j=1,2,\ldots,L}$, the configuration $\{e^{i\theta}\alpha_j, e^{-i\theta}\beta_j\}_{j=1,2,\ldots,L}$ is also a minimum for any value of θ. To simplify the derivation, let us take $\theta = 0$ as the representative minimum, specifically taking α_j and β_j real and positive. The minimization conditions $\partial E/\partial\alpha_j = 0 = \partial E/\partial\beta_j$ read now

$$(U\alpha_j^2 - \mu)\alpha_j + V\alpha_j(\alpha_{j+1}^2 + \alpha_{j-1}^2) = J(\alpha_{j+1} + \alpha_{j-1}) + \varepsilon\beta_j, \tag{25a}$$

$$(U\beta_j^2 - \mu)\beta_j + V\beta_j(\beta_{j+1}^2 + \beta_{j-1}^2) = J(\beta_{j+1} + \beta_{j-1}) + \varepsilon\alpha_j. \tag{25b}$$

These equations possess balanced solutions with $\alpha_j = \beta_j$ as well as unbalanced ones with $\alpha_j \neq \beta_j$. The variational energy of the balanced ones is equal to twice the one we studied in the preceding section for the previous model, Eq. (13). Hence, such balanced configurations have the same energy landscape and phase diagram as the one we studied in the previous case. Specifically, a homogeneous solution dominates when $V/U \leqslant 1/2 + 1/\nu$, with $\nu = (\mu + \varepsilon)/2J$, while a staggered solution appears when $V/U > 1/2 + 1/\nu$. Hence, the coherent-state ansatz predicts a transition from a homogeneous superfluid to a supersolid phase in the balanced sector, in both cases breaking a continuous U(1) symmetry spontaneously.

It is possible to find analytically or semianalytically unbalanced solutions to (25), as we show in Appendix E. Moreover, in that same Appendix we explain how we have used imaginary-time dynamics to perform an exhaustive numerical search of other local minima. In all cases, we have found that the balanced solutions have always lower energy than the unbalanced ones.

These results provide solid arguments that show that it is possible to extend the model studied in the previous sec-

tions in such a way that pair injection retains a full U(1) symmetry while still leading to the same enhancement of supersolidity in the phase diagram.

VII. CONNECTION OF OUR WORK TO DRIVEN-DISSIPATIVE EXPERIMENTAL PLATFORMS

In previous sections we have studied the ground state of the extended Bose-Hubbard Hamiltonian onto which we add a coherent pair injection term $-\varepsilon(\hat{a}_j^2 + \hat{a}_j^{\dagger 2})/2$ at each lattice site j. The motivation behind our study comes from the fact that such a process is accessible in modern experimental quantum simulation platforms such as superconducting circuits [32–34,37–40], photonic devices [15,16,19,60], and even cold atoms [61–66]. However, our description based on adding that time-independent Hamiltonian is a simplification, not aimed at truly modeling experiments, but just at understanding the generic effect of ε, in particular proving that it favors supersolidity. Here we introduce a more rigorous theoretical model for pair injection as implemented in experiments and connect it to our simplified description.

Our starting point is a system consisting of a set of identical bosonic modes with characteristic energy ω_0. In an experiment, these can correspond, for example, to the microwave modes of a superconducting circuit [5,20–26], the photonic modes of an optical cavity array [16,67], or the Wannier modes of cold atoms trapped in optical lattices [2,13,14]. In these experimental platforms ω_0 is usually the dominant energy scale, so any other processes such as hopping or interactions are implemented effectively as some sort of perturbation. We thus assume that a model including all the particle-conserving terms present on the extended Bose-Hubbard Hamiltonian has been implemented in such a platform:

$$\hat{H}_0 = \sum_j \left(\omega_0\hat{n}_j + \frac{U}{2}\hat{n}_j(\hat{n}_j - 1) \right.$$
$$\left. - J(\hat{a}_j^\dagger\hat{a}_{j+1} + \hat{a}_{j+1}^\dagger\hat{a}_j) + V\hat{n}_{j+1}\hat{n}_j \right). \tag{26}$$

Let us remark that at this point, ω_0 does not have the significance of a chemical potential and is the scale that dominates over the rest $\omega_0 \gg J, U, V$. However, we will show shortly that an effective chemical potential on the scale of the rest of parameters appears in these systems when driven by an external field.

Let us now explain how coherent pair injection is implemented on these systems. Being a particle nonconserving process, it requires coupling the system to some sort of environment from which we can feed and extract excitations. This implies that, in general, the description of the system has to be made in terms of a mixed state $\hat{\rho}$ rather than a pure one [44,68–70] (since correlations emerge with the environment), which will then be subjected to both driving and dissipation. In Appendix F we provide a generic description for such a system plus environment model and rigorously integrate out the environment under standard Born-Markov assumptions [44,68–70] to find a dynamical equation for the state of the system alone. The resulting system dynamics is governed by

a so-called master equation that reads

$$\partial_t \hat{\rho} = -i[\hat{H}(t), \hat{\rho}] + \sum_j \gamma (2\hat{a}_j^2 \hat{\rho} \hat{a}_j^{\dagger 2} - \hat{a}_j^{\dagger 2} \hat{a}_j^2 \hat{\rho} - \hat{\rho} \hat{a}_j^{\dagger 2} \hat{a}_j^2)$$

$$+ \sum_j \kappa (2\hat{a}_j \hat{\rho} \hat{a}_j^{\dagger} - \hat{a}_j^{\dagger} \hat{a}_j \hat{\rho} - \hat{\rho} \hat{a}_j^{\dagger} \hat{a}_j), \qquad (27)$$

with the time-dependent Hamiltonian

$$\hat{H}(t) = \hat{H}_0 - \sum_j \frac{\varepsilon}{2} (e^{-2i\omega_d t} \hat{a}_j^{\dagger 2} + e^{2i\omega_d t} \hat{a}_j^2). \qquad (28)$$

Here γ and κ are real and positive and we assume the same for ε for definiteness. Driving corresponds to the time-dependent term of (28), where $\varepsilon \ll \omega_0$ provides the rate at which an external drive at tunable frequency $2\omega_d$ exchanges pairs of excitations with the system through the environment; in order for this term to play a role, $|\omega_d - \omega_0|$ must not be much larger than the driving rate ε, as otherwise it is highly suppressed by energy conservation (rotating-wave or secular approximation [44]). The coupling to the environment has another important effect, corresponding to the second and third terms in (27): the incoherent loss of system excitations, either individually at rate κ or by pairs at rate γ. In particular, the terms $\hat{a}_j \hat{\rho} \hat{a}_j^{\dagger}$ and $\hat{a}_j^2 \hat{\rho} \hat{a}_j^{\dagger 2}$ effect random quantum jumps removing one or two excitations at a time, respectively [44]. It is important to remark that each of these terms comes from a different environment and hence they are independent (see Appendix F for more details).

Hence, experiments deal with a driven-dissipative problem that deviates from the problem that we have analyzed in the previous sections in two ways. First, the Hamiltonian is time dependent. This, however, is avoided by moving to a picture rotating at frequency ω_d. The state in the new picture is $\hat{\rho}_R = \hat{R}^{\dagger}(t)\hat{\rho}\hat{R}(t)$, with $\hat{R} = \exp(-i\omega_d t \hat{N})$, where $\hat{N} = \sum_j \hat{a}_j^{\dagger} \hat{a}_j$ is the total number operator. This state is easily shown [44] to evolve according to the same master equation (27) but with a time-independent Hamiltonian

$$\hat{H}_R = e^{i\omega_d t \hat{N}}[\hat{H}(t) - \omega_d \hat{N}]e^{-i\omega_d t \hat{N}}$$

$$= \sum_j \left((\omega_0 - \omega_d)\hat{n}_j - \frac{\varepsilon}{2}(\hat{a}_j^2 + \hat{a}_j^{\dagger 2}) + \frac{U}{2}\hat{n}_j(\hat{n}_j - 1) \right.$$

$$\left. - J(\hat{a}_j^{\dagger}\hat{a}_{j+1} + \hat{a}_{j+1}^{\dagger}\hat{a}_j) + V\hat{n}_{j+1}\hat{n}_j \right), \qquad (29)$$

where we have used $\hat{R}^{\dagger}(t)\hat{a}\hat{R}(t) = e^{-i\omega_d t}\hat{a}$. This is precisely the Hamiltonian that we have used throughout. Note that an effective chemical potential $\mu = \omega_d - \omega_0$ emerges in this type of driven-dissipative experiments, which can be controlled via the detuning between the driving frequency ω_d and the characteristic energy ω_0 of the bosonic modes.

The presence of dissipation at rate γ is the second way in which the experiments deviate from the situation that we have analyzed herein, in which we have just considered the Hamiltonian part. In general, the interplay between the Hamiltonian and dissipation will make the system settle into some kind of steady state defined by $\partial_t \hat{\rho}_R = 0$; finding such a state should be the ultimate goal of any theoretical approach aiming at making precise experimental predictions. Unfortu-

nately, being a many-body driven-dissipative problem, this is an exceedingly hard task. However, it is well known in the few-body realm of quantum optics that the properties of such steady states are typically inherited from the properties found in the Hamiltonian when dissipative processes involved are of the simple type we deal here with. For example, Hamiltonian systems possessing squeezed ground states in the rotating picture lead to squeezed mixed steady states when dissipation is added [44,71]. Hence, understanding the effect that pair injection has on the phases of the system's rotating-picture Hamiltonian is a crucial step in determining the type of steady states that will be available via dissipative state preparation. In our case, we have shown that supersolid states are favored at the Hamiltonian level, so our work suggests that pair injection should help stabilizing supersolid phases in driven-dissipative setups. We plan on proving this statement rigorously in the near future by applying stochastic phase-space techniques [72–74] to the master equation (27).

VIII. CONCLUSION

As a first step towards understanding its effect on quantum simulators, we have analyzed how coherent pair injection affects the ground-state phase diagram of the extended Bose-Hubbard model. We have shown that it favors supersolid order over both insulating and homogeneous superfluid order, albeit in a model with Z_2 symmetry. However, our results have been shown to be extensible to models with U(1) symmetry. Driven-dissipative quantum optical platforms have become the focus of intense research in recent decades due to their potential for realizing unexplored many-body models. Regarding our model, we have pointed out that the injection term usually comes from some sort of external field that ultimately leads to dissipation [75,76]. Nevertheless, the interplay between coherent and dissipative processes makes the system settle into a nonequilibrium (steady) state that typically inherits properties from the Hamiltonian [44,71]. Hence, we hope that our work, which proves that pair injection provides a controllable knob to access supersolid phases, will trigger further effort in the stabilization of supersolidity as a steady state through a dissipative phase transition [77–82].

APPENDIX A: GROUND STATE IN THE $J = 0 = \varepsilon$ LIMIT

Our work focuses on the analysis of the ground-state properties of the Hamiltonian (1). While no analytic solution exists
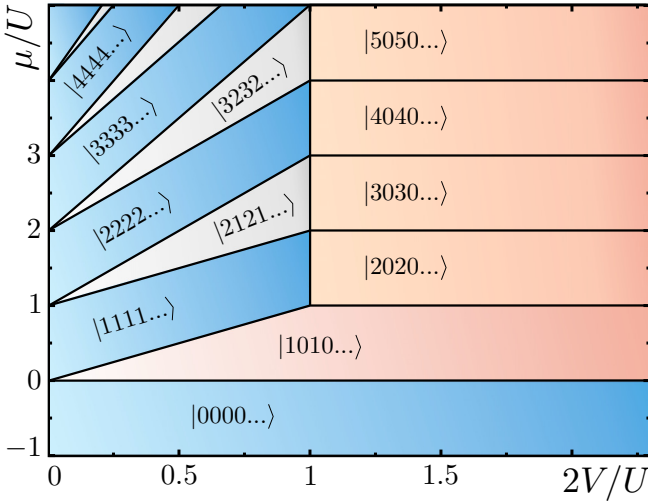
FIG. 5. Phase diagram of the $J = 0 = \varepsilon$ model (extended Bose-Hubbard model at zero hopping). The labels of the states refer to the Fock numbers on each lattice site, that is, $\bigotimes_{j=1}^{L/2} |\bar{n}_o\rangle \otimes |\bar{n}_e\rangle = |n_1 n_2 n_3 n_4 \cdots\rangle$, as given by (A1).

for this problem in all parameter space, it is interesting to consider the $J = 0 = \varepsilon$ limit, where the problem is readily solvable. In this limit, the Hamiltonian depends solely on number operators $\hat{n}_j$, so it is diagonalized in the Fock basis $\{\bigotimes_{j=1}^{L} |n_j\rangle\}_{n_j=0,1,2,\ldots}$, with $\hat{n}_j|n\rangle = n|n\rangle$. It is not difficult to

show that the ground state is given by alternating Fock numbers, particularly $\bigotimes_{j=1}^{L/2} |\bar{n}_o\rangle \otimes |\bar{n}_e\rangle$, with

$$\bar{n}_o = \begin{cases} \left\lceil \frac{\mu}{U} \right\rceil & \text{for } 2V/U > 1 \\ \left\lceil \frac{\mu}{U+2V} \right\rceil & \text{for } 2V/U < 1, \end{cases} \quad \text{(A1a)}$$

$$\bar{n}_e = \begin{cases} 0 & \text{for } 2V/U > 1 \\ \left\lceil \frac{\mu - 2V}{U+2V} \right\rceil & \text{for } 2V/U < 1, \end{cases} \quad \text{(A1b)}$$

where $\lceil x \rceil$ is the ceiling function, which corresponds to the smallest integer not smaller than x. Of course, owed to the translational invariance of the model, the state $\bigotimes_{j=1}^{L/2} |\bar{n}_e\rangle \otimes |\bar{n}_o\rangle$ has the same energy, but we take the density of odd sites larger than that of even sites for definiteness. We represent the ground state in the $(2V/U, \mu/U)$ phase diagram in Fig. 5.

APPENDIX B: MORE ON THE MEAN-FIELD APPROXIMATION

We start this Appendix providing the ground-state phase diagrams built from the raw numerical data that we obtained with the MF approach (self-consistent Hartree-Fock) that we introduced in Sec. IV. We present them in Fig. 6, where they are seen to coincide with less smooth versions of those of Fig. 1.

In addition, for $\varepsilon = 0$ it is possible to find the boundaries between insulating (MI or DW) and superfluid (SF or SS) phases analytically. In short, the idea is to interpret the MF
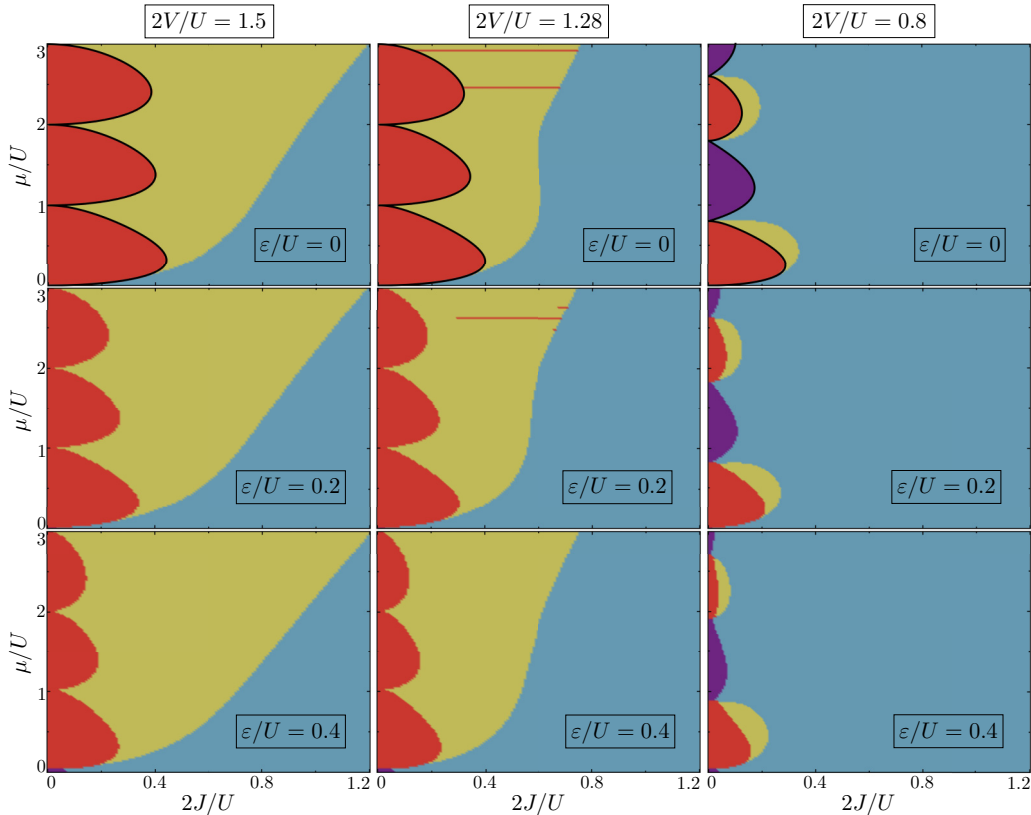

FIG. 6. Numerical MF phase diagrams (blue denotes SF; yellow, SS; red, DW; and purple, MI). The thick black line in the top row corresponds to the analytical perturbative expression for the insulating-superfluid boundary [Eq. (B15)].

approximation to $E = \langle \hat{H} \rangle$ as sort of a Landau potential that depends on the complex parameters $\boldsymbol{\phi} = (\phi_{\rm o}, \phi_{\rm e})^{\sf T}$ that we collect into a column vector for later convenience. In the insulating phases, the potential has a minimum at $\boldsymbol{\phi} = 0$, but this minimum flattens out as the boundary towards the superfluid phases is approached, until it becomes unstable once we cross it and new minima emerge at $\boldsymbol{\phi} \neq 0$. Hence, in this Appendix we let the parameters $\boldsymbol{\phi}$ of the MF Hamiltonian vary freely, using them as Landau order parameters and seeking the points of the phase diagram at which the curvature of $E(\boldsymbol{\phi})$ vanishes. This will provide analytic expressions for the insulating-superfluid boundary. Note that throughout this Appendix the other MF parameters keep their $\rho_j = \langle \hat{n}_j \rangle$ definition. Let us now elaborate on the details of this procedure.

Given the MF variational ansatz $\bigotimes_{j=1}^{L/2} |\psi_{\rm o}\rangle \otimes |\psi_{\rm e}\rangle$, we begin by defining the variational energy per pair of sites associated with the Hamiltonian (1),

$$
\begin{aligned}
e = \frac{\langle \hat{H} \rangle}{L/2} = {}& -\mu(\langle \hat{n}_{\rm o} \rangle + \langle \hat{n}_{\rm e} \rangle) + \frac{U}{2}[\langle \hat{n}_{\rm o}(\hat{n}_{\rm o} - 1) \rangle \\
& + \langle \hat{n}_{\rm e}(\hat{n}_{\rm e} - 1) \rangle] - 2J(\langle \hat{a}_{\rm o}^\dagger \rangle \langle \hat{a}_{\rm e} \rangle \\
& + \langle \hat{a}_{\rm e}^\dagger \rangle \langle \hat{a}_{\rm o} \rangle) + 2V \langle \hat{n}_{\rm o} \rangle \langle \hat{n}_{\rm e} \rangle.
\end{aligned} \tag{B1}
$$

Similarly, writing the MF Hamiltonian per pair of sites from (8) and (11) as

$$
\begin{aligned}
\hat{h}_{\rm MF} \equiv \frac{\hat{H}_{\rm MF}}{L/2} = {}& -\mu(\hat{n}_{\rm o} + \hat{n}_{\rm e}) + \frac{U}{2}[\hat{n}_{\rm o}(\hat{n}_{\rm o} - 1) + \hat{n}_{\rm e}(\hat{n}_{\rm e} - 1)] \\
& + 2V(\langle \hat{n}_{\rm e} \rangle \hat{n}_{\rm o} + \langle \hat{n}_{\rm o} \rangle \hat{n}_{\rm e} - \langle \hat{n}_{\rm o} \rangle \langle \hat{n}_{\rm e} \rangle) \\
& - 2J(\phi_{\rm e}^* \hat{a}_{\rm o} + \phi_{\rm e} \hat{a}_{\rm o}^\dagger + \phi_{\rm o}^* \hat{a}_{\rm e} + \phi_{\rm o} \hat{a}_{\rm e}^\dagger - \phi_{\rm o}^* \phi_{\rm e} \\
& - \phi_{\rm e}^* \phi_{\rm o}),
\end{aligned} \tag{B2}
$$

we can define the MF energy per pair of sites as

$$
e_{\rm MF} \equiv \langle \hat{h}_{\rm MF} \rangle \tag{B3}
$$

$$
\begin{aligned}
= {}& -\mu(\langle \hat{n}_{\rm o} \rangle + \langle \hat{n}_{\rm e} \rangle) \\
& + \frac{U}{2}[\langle \hat{n}_{\rm o}(\hat{n}_{\rm o} - 1) \rangle + \langle \hat{n}_{\rm e}(\hat{n}_{\rm e} - 1) \rangle] + 2V \langle \hat{n}_{\rm o} \rangle \langle \hat{n}_{\rm e} \rangle \\
& - 2J(\phi_{\rm e}^* \langle \hat{a}_{\rm o} \rangle + \phi_{\rm e} \langle \hat{a}_{\rm o}^\dagger \rangle + \phi_{\rm o}^* \langle \hat{a}_{\rm e} \rangle + \phi_{\rm o} \langle \hat{a}_{\rm e}^\dagger \rangle \\
& - \phi_{\rm o}^* \phi_{\rm e} - \phi_{\rm e}^* \phi_{\rm o}).
\end{aligned} \tag{B4}
$$

We then have the following relation between the variational energy and the MF energy:

$$
e = e_{\rm MF} - 2J[(\langle \hat{a}_{\rm o} \rangle^* - \phi_{\rm o}^*)(\langle \hat{a}_{\rm e} \rangle - \phi_{\rm e}) + {\rm c.c.}]. \tag{B5}
$$

The goal is to relate e to $\boldsymbol{\phi}$ and then check its curvature at $\boldsymbol{\phi} = 0$, which is built from the second-order derivatives $\mathcal{K}_{jk} = \partial^2 e / \partial \phi_j \partial \phi_k |_{\boldsymbol{\phi}=0}$. Hence, we do not care about the full dependence of e on $\boldsymbol{\phi}$, but just about its quadratic expansion around $\boldsymbol{\phi} = 0$. This is consistent with performing second-order perturbation theory in J on $\hat{h}_{\rm MF}$, which indeed leads to a quadratic form in $\boldsymbol{\phi}$, as we show next. Moreover, recall from Appendix A that for $J = 0 = \varepsilon$ we know the exact eigenstates of $\hat{H}$ and they have $\langle \hat{a}_j \rangle = 0$, so J is precisely the parameter that brings in the coherence $\boldsymbol{\phi} \neq 0$. However, applying perturbation theory to $\hat{h}_{\rm MF}$ is not as straightforward as it might seem, since it is a function of $\langle \hat{n}_j \rangle$, so it defines a nonlinear eigenproblem, where the operator we want to

diagonalize depends on its eigenstates. We carefully perform such perturbation theory at the end of this Appendix, but here we just provide the final result for the ground-state energy, which reads

$$
\begin{aligned}
e_{\rm MF}(\boldsymbol{\phi}) \approx {}& e_{\bar{n}_{\rm o} \bar{n}_{\rm e}}^{(0)} + 2J(\phi_{\rm o}^* \phi_{\rm e} + \phi_{\rm o} \phi_{\rm e}^*) \\
& - \frac{4J^2}{U} \chi_{\rm o} |\phi_{\rm e}|^2 - \frac{4J^2}{U} \chi_{\rm e} |\phi_{\rm o}|^2,
\end{aligned} \tag{B6}
$$

where

$$
\begin{aligned}
e_{\bar{n}_{\rm o} \bar{n}_{\rm e}}^{(0)} = {}& -\mu(\bar{n}_{\rm o} + \bar{n}_{\rm e}) + 2V \bar{n}_{\rm o} \bar{n}_{\rm e} \\
& + \frac{U}{2}[\bar{n}_{\rm o}(\bar{n}_{\rm o} - 1) + \bar{n}_{\rm e}(\bar{n}_{\rm e} - 1)]
\end{aligned} \tag{B7}
$$

is the ground-state energy of the system in the $J = 0$ limit, with $\{\bar{n}_j\}_{j={\rm o,e}}$ given by (A1), and

$$
\chi_{\rm o} = \frac{\bar{n}_{\rm o}}{\mu/U - 2\bar{n}_{\rm e}V/U + 1 - \bar{n}_{\rm o}} + \frac{\bar{n}_{\rm o} + 1}{\bar{n}_{\rm o} - \mu/U + 2\bar{n}_{\rm e}V/U}, \tag{B8a}
$$

$$
\chi_{\rm e} = \frac{n_{\rm e}}{\mu/U - 2\bar{n}_{\rm o}V/U + 1 - \bar{n}_{\rm e}} + \frac{\bar{n}_{\rm e} + 1}{\bar{n}_{\rm e} - \mu/U + 2\bar{n}_{\rm o}V/U}. \tag{B8b}
$$

Note that $\chi_j \geq 0$.

In order to turn the variational energy per pair of sites e of Eq. (B5) into a function of $\boldsymbol{\phi}$, we also have to relate the expectation values $\langle \hat{a}_j \rangle$ to $\boldsymbol{\phi}$. We do this by considering the Hellmann-Feynman theorem [83] within the MF approximation, which states that

$$
\frac{\partial e_{\rm MF}}{\partial \phi_j} = \left\langle \frac{\partial \hat{h}_{\rm MF}}{\partial \phi_j} \right\rangle. \tag{B9}
$$

Evaluating the right-hand side from (B2) and the left-hand side from (B6), we obtain

$$
\langle \hat{a}_{\rm o} \rangle = \frac{2J}{U} \chi_{\rm o} \phi_{\rm e}, \tag{B10a}
$$

$$
\langle \hat{a}_{\rm e} \rangle = \frac{2J}{U} \chi_{\rm e} \phi_{\rm o} \tag{B10b}
$$

to leading order in J. Putting expressions (B6) and (B10) together in (B5) and keeping terms only up to quadratic order in $\boldsymbol{\phi}$, we obtain the quadratic form

$$
\begin{aligned}
e &\approx e_{\bar{n}_{\rm o} \bar{n}_{\rm e}}^{(0)} + \frac{4J^2}{U}[\chi_{\rm e}|\phi_{\rm o}|^2 + \chi_{\rm o}|\phi_{\rm e}|^2 - 2J\chi_{\rm o}\chi_{\rm e}(\phi_{\rm e}^* \phi_{\rm o} + \phi_{\rm e}\phi_{\rm o}^*)] \\
&= e_{\bar{n}_{\rm o} \bar{n}_{\rm e}}^{(0)} + \boldsymbol{\phi}^\dagger \mathcal{K} \boldsymbol{\phi},
\end{aligned} \tag{B11}
$$

with the real symmetric curvature matrix

$$
\mathcal{K} = \frac{4J^2}{U} \begin{pmatrix} \chi_{\rm e} & -2J\chi_{\rm o}\chi_{\rm e}/U \\ -2J\chi_{\rm o}\chi_{\rm e}/U & \chi_{\rm o} \end{pmatrix}. \tag{B12}
$$

We can diagonalize the curvature matrix as $\mathcal{K} = \mathcal{S}^{\sf T} {\rm diag}(\kappa_+, \kappa_-)\mathcal{S}$, where $\mathcal{S}$ is an orthonormal matrix (whose specific form is irrelevant for our purposes) and the eigenvalues read

$$
\kappa_\pm = \frac{2J^2}{U}\left[\chi_{\rm e} + \chi_{\rm o} \pm \sqrt{(\chi_{\rm e} - \chi_{\rm o})^2 + 16J^2\chi_{\rm o}^2\chi_{\rm e}^2/U^2}\right]. \tag{B13}
$$

Defining then new complex parameters $(\phi_+, \phi_-)^{\mathsf{T}} = \mathcal{S}\boldsymbol{\phi}$, the Landau potential $e(\boldsymbol{\phi})$ can be written as

$$e(\boldsymbol{\phi}) \approx e_0 + \kappa_+|\phi_+|^2 + \kappa_-|\phi_-|^2. \qquad (B14)$$

Therefore, the condition for stability of the $\boldsymbol{\phi} = 0$ configuration is $\kappa_\pm > 0$ (which $J = 0$ satisfies), while as soon as the curvature κ_- turns negative, that trivial configuration becomes unstable (which happens for sufficiently large J). Hence, the boundary between insulator and superfluid phases is determined by the condition

$$\kappa_- = 0 \iff \frac{J}{U} = \frac{1}{2\sqrt{\chi_{\mathrm{o}}\chi_{\mathrm{e}}}}. \qquad (B15)$$

As shown in Fig. 6, this simple analytic condition fits perfectly the insulating-superfluid boundaries found via the self-consistent Hartree-Fock procedure in Appendix A.

To end this Appendix we prove Eq. (B6) by developing a perturbative solution to the nonlinear eigenproblem defined by $\hat{h}_{\mathrm{MF}}(\langle\hat{n}_{\mathrm{o}}\rangle, \langle\hat{n}_{\mathrm{e}}\rangle)$. We start by writing the Hamiltonian as $\hat{h}_{\mathrm{MF}} = \hat{h}_0 + \hat{w}$, where

$$\begin{aligned}
\hat{h}_0 &= (-\mu + 2V\langle\hat{n}_{\mathrm{e}}\rangle_{J=0})\hat{n}_{\mathrm{o}} + (-\mu + 2V\langle\hat{n}_{\mathrm{o}}\rangle_{J=0})\hat{n}_{\mathrm{e}} \\
&\quad + \frac{U}{2}[\hat{n}_{\mathrm{o}}(\hat{n}_{\mathrm{o}} - 1) + \hat{n}_{\mathrm{e}}(\hat{n}_{\mathrm{e}} - 1)] - 2V\langle\hat{n}_{\mathrm{o}}\rangle_{J=0}\langle\hat{n}_{\mathrm{e}}\rangle_{J=0}
\end{aligned} \qquad (B16)$$

is the MF Hamiltonian per pair of sites at $J = 0$, which we take as our unperturbed Hamiltonian, and

$$\begin{aligned}
\hat{w} &= -2J(\phi_{\mathrm{e}}^*\hat{a}_{\mathrm{o}} + \phi_{\mathrm{e}}\hat{a}_{\mathrm{o}}^\dagger + \phi_{\mathrm{o}}^*\hat{a}_{\mathrm{e}} + \phi_{\mathrm{o}}\hat{a}_{\mathrm{e}}^\dagger - \phi_{\mathrm{o}}^*\phi_{\mathrm{e}} - \phi_{\mathrm{e}}^*\phi_{\mathrm{o}}) \\
&\quad + 2V[(\langle\hat{n}_{\mathrm{e}}\rangle - \langle\hat{n}_{\mathrm{e}}\rangle_{J=0})\hat{n}_{\mathrm{o}} + (\langle\hat{n}_{\mathrm{o}}\rangle - \langle\hat{n}_{\mathrm{o}}\rangle_{J=0})\hat{n}_{\mathrm{e}} \\
&\quad - (\langle\hat{n}_{\mathrm{o}}\rangle\langle\hat{n}_{\mathrm{e}}\rangle - \langle\hat{n}_{\mathrm{o}}\rangle_{J=0}\langle\hat{n}_{\mathrm{e}}\rangle_{J=0})]
\end{aligned} \qquad (B17)$$

is the perturbation. Even though $\hat{h}_0$ defines also a nonlinear problem, its eigenstates are trivially found to be the Fock states $\{|n_{\mathrm{o}}, n_{\mathrm{e}}\rangle \equiv |n_{\mathrm{o}}\rangle \otimes |n_{\mathrm{e}}\rangle\}_{n_j=0,1,2,\ldots}$, as it depends solely on number operators. We thus have $\hat{h}_0|n_{\mathrm{o}}, n_{\mathrm{e}}\rangle = e_{n_{\mathrm{o}}n_{\mathrm{e}}}^{(0)}|n_{\mathrm{o}}, n_{\mathrm{e}}\rangle$, with

$$\begin{aligned}
e_{n_{\mathrm{o}}n_{\mathrm{e}}}^{(0)} &= -\mu(n_{\mathrm{o}} + n_{\mathrm{e}}) + 2Vn_{\mathrm{o}}n_{\mathrm{e}} + \frac{U}{2}[n_{\mathrm{o}}(n_{\mathrm{o}} - 1) \\
&\quad + n_{\mathrm{e}}(n_{\mathrm{e}} - 1)].
\end{aligned} \qquad (B18)$$

These coincide with the eigenenergies of the full Hamiltonian per pair of sites $\hat{H}/(L/2)$ for $J = 0 = \varepsilon$. Hence, $|\bar{n}_{\mathrm{o}}, \bar{n}_{\mathrm{e}}\rangle$, with Fock numbers provided by (A1), is the ground state of $\hat{h}_0$. We already found that this ground-state energy has a degeneracy related to the translational invariance of the model. In addition, for $2V > U$ it is also degenerate when μ/U is a positive integer or zero, leading to the same energies for $|\bar{n}_{\mathrm{o}}, 0\rangle$ and $|\bar{n}_{\mathrm{o}} + 1, 0\rangle$. Similarly, for $2V < U$ the degeneracy appears when $\mu/(U + 2V)$ is a positive integer or zero. Nevertheless, we will see that nondegenerate perturbation theory gives sensible results even at those degeneracy points, so there is no need to treat them separately with degenerate perturbation theory.

We consider the full MF eigenproblem

$$\hat{h}_{\mathrm{MF}}|\psi_{n_{\mathrm{o}}n_{\mathrm{e}}}\rangle = e_{n_{\mathrm{o}}n_{\mathrm{e}}}|\psi_{n_{\mathrm{o}}n_{\mathrm{e}}}\rangle \qquad (B19)$$

and assume as usual in perturbation theory that the eigenstates and eigenenergies admit a series expansion in J,

$$|\psi_{n_{\mathrm{o}}n_{\mathrm{e}}}\rangle = |n_{\mathrm{o}}, n_{\mathrm{e}}\rangle + J|\psi_{n_{\mathrm{o}}n_{\mathrm{e}}}^{(1)}\rangle + J^2|\psi_{n_{\mathrm{o}}n_{\mathrm{e}}}^{(2)}\rangle + \cdots, \quad (B20a)$$

$$e_{n_{\mathrm{o}}n_{\mathrm{e}}} = e_{n_{\mathrm{o}}n_{\mathrm{e}}}^{(0)} + Je_{n_{\mathrm{o}}n_{\mathrm{e}}}^{(1)} + J^2e_{n_{\mathrm{o}}n_{\mathrm{e}}}^{(2)} + \cdots. \qquad (B20b)$$

As we will see, we can choose $\langle n_{\mathrm{o}}, n_{\mathrm{e}}|\psi_{n_{\mathrm{o}}n_{\mathrm{e}}}^{(1)}\rangle \in \mathbb{R}$. Moreover, we can demand that the eigenstates are normalized at all orders so that

$$1 = \langle\psi_{n_{\mathrm{o}}n_{\mathrm{e}}}|\psi_{n_{\mathrm{o}}n_{\mathrm{e}}}\rangle \qquad (B21)$$

$$\begin{aligned}
&= \overbrace{\langle n_{\mathrm{o}}, n_{\mathrm{e}}|n_{\mathrm{o}}, n_{\mathrm{e}}\rangle}^{1} + J(\langle n_{\mathrm{o}}, n_{\mathrm{e}}|\psi_{n_{\mathrm{o}}n_{\mathrm{e}}}^{(1)}\rangle + \langle\psi_{n_{\mathrm{o}}n_{\mathrm{e}}}^{(1)}|n_{\mathrm{o}}, n_{\mathrm{e}}\rangle) \\
&\quad + J^2(\langle\psi_{n_{\mathrm{o}}n_{\mathrm{e}}}^{(1)}|\psi_{n_{\mathrm{o}}n_{\mathrm{e}}}^{(1)}\rangle + \langle n_{\mathrm{o}}, n_{\mathrm{e}}|\psi_{n_{\mathrm{o}}n_{\mathrm{e}}}^{(2)}\rangle + \langle\psi_{n_{\mathrm{o}}n_{\mathrm{e}}}^{(2)}|n_{\mathrm{o}}, n_{\mathrm{e}}\rangle) \\
&\quad + \cdots
\end{aligned} \qquad (B22)$$

implies

$$\langle n_{\mathrm{o}}, n_{\mathrm{e}}|\psi_{n_{\mathrm{o}}n_{\mathrm{e}}}^{(1)}\rangle = 0, \qquad (B23a)$$

$$\langle n_{\mathrm{o}}, n_{\mathrm{e}}|\psi_{n_{\mathrm{o}}n_{\mathrm{e}}}^{(2)}\rangle + \langle\psi_{n_{\mathrm{o}}n_{\mathrm{e}}}^{(2)}|n_{\mathrm{o}}, n_{\mathrm{e}}\rangle = -\langle\psi_{n_{\mathrm{o}}n_{\mathrm{e}}}^{(1)}|\psi_{n_{\mathrm{o}}n_{\mathrm{e}}}^{(1)}\rangle. \quad (B23b)$$

These expressions will be useful later. Next we evaluate the expectation values appearing in the Hamiltonian,

$$\begin{aligned}
\langle\hat{n}_j\rangle &= \overbrace{\langle n_{\mathrm{o}}, n_{\mathrm{e}}|\hat{n}_j|n_{\mathrm{o}}, n_{\mathrm{e}}\rangle}^{n_j=\langle\hat{n}_j\rangle_{J=0}} + J\Big(\overbrace{\langle n_{\mathrm{o}}, n_{\mathrm{e}}|\hat{n}_j|\psi_{n_{\mathrm{o}}n_{\mathrm{e}}}^{(1)}\rangle}^{n_j\langle n_{\mathrm{o}}, n_{\mathrm{e}}|\psi_{n_{\mathrm{o}}n_{\mathrm{e}}}^{(1)}\rangle=0} \\
&\quad + \overbrace{\langle\psi_{n_{\mathrm{o}}n_{\mathrm{e}}}^{(1)}|\hat{n}_j|n_{\mathrm{o}}, n_{\mathrm{e}}\rangle}^{n_j\langle\psi_{n_{\mathrm{o}}n_{\mathrm{e}}}^{(1)}|n_{\mathrm{o}}, n_{\mathrm{e}}\rangle=0}\Big) + J^2\big(\langle\psi_{n_{\mathrm{o}}n_{\mathrm{e}}}^{(1)}|\hat{n}_j|\psi_{n_{\mathrm{o}}n_{\mathrm{e}}}^{(1)}\rangle \\
&\quad + \underbrace{\langle n_{\mathrm{o}}, n_{\mathrm{e}}|\hat{n}_j|\psi_{n_{\mathrm{o}}n_{\mathrm{e}}}^{(2)}\rangle + \langle\psi_{n_{\mathrm{o}}n_{\mathrm{e}}}^{(2)}|\hat{n}_j|n_{\mathrm{o}}, n_{\mathrm{e}}\rangle}_{-n_j\langle\psi_{n_{\mathrm{o}}n_{\mathrm{e}}}^{(1)}|\psi_{n_{\mathrm{o}}n_{\mathrm{e}}}^{(1)}\rangle}\big) + \cdots,
\end{aligned} \qquad (B24)$$

so

$$\langle\hat{n}_j\rangle - \langle\hat{n}_j\rangle_{J=0} = J^2\langle\psi_{n_{\mathrm{o}}n_{\mathrm{e}}}^{(1)}|(\hat{n}_j - n_j)|\psi_{n_{\mathrm{o}}n_{\mathrm{e}}}^{(1)}\rangle + \cdots, \qquad (B25a)$$

$$\begin{aligned}
\langle\hat{n}_{\mathrm{o}}\rangle\langle\hat{n}_{\mathrm{e}}\rangle - \langle\hat{n}_{\mathrm{o}}\rangle_{J=0}\langle\hat{n}_{\mathrm{e}}\rangle_{J=0} &= J^2\big[n_{\mathrm{o}}\langle\psi_{n_{\mathrm{o}}n_{\mathrm{e}}}^{(1)}|(\hat{n}_{\mathrm{e}} - n_{\mathrm{e}})|\psi_{n_{\mathrm{o}}n_{\mathrm{e}}}^{(1)}\rangle \\
&\quad + n_{\mathrm{e}}\langle\psi_{n_{\mathrm{o}}n_{\mathrm{e}}}^{(1)}|(\hat{n}_{\mathrm{o}} - n_{\mathrm{o}})|\psi_{n_{\mathrm{o}}n_{\mathrm{e}}}^{(1)}\rangle\big] \\
&\quad + \cdots.
\end{aligned} \qquad (B25b)$$

It is then convenient to split the perturbation as $\hat{w} = J\hat{h} + J^2\hat{v}$, with

$$\hat{h} = -2(\phi_{\mathrm{e}}^*\hat{a}_{\mathrm{o}} + \phi_{\mathrm{e}}\hat{a}_{\mathrm{o}}^\dagger + \phi_{\mathrm{o}}^*\hat{a}_{\mathrm{e}} + \phi_{\mathrm{o}}\hat{a}_{\mathrm{e}}^\dagger - \phi_{\mathrm{o}}^*\phi_{\mathrm{e}} - \phi_{\mathrm{e}}^*\phi_{\mathrm{o}}), \qquad (B26a)$$

$$\begin{aligned}
\hat{v} &= 2V\big[\langle\psi_{n_{\mathrm{o}}n_{\mathrm{e}}}^{(1)}|(\hat{n}_{\mathrm{e}} - n_{\mathrm{e}})|\psi_{n_{\mathrm{o}}n_{\mathrm{e}}}^{(1)}\rangle(\hat{n}_{\mathrm{o}} - n_{\mathrm{o}}) \\
&\quad + \langle\psi_{n_{\mathrm{o}}n_{\mathrm{e}}}^{(1)}|(\hat{n}_{\mathrm{o}} - n_{\mathrm{o}})|\psi_{n_{\mathrm{o}}n_{\mathrm{e}}}^{(1)}\rangle(\hat{n}_{\mathrm{e}} - n_{\mathrm{e}})\big],
\end{aligned} \qquad (B26b)$$

so that the MF Hamiltonian is written as

$$\hat{h}_{\mathrm{MF}} = \hat{h}_0 + J\hat{h} + J^2\hat{v}, \qquad (B27)$$

with all terms showing explicitly the order in J to which they contribute. Inserting (B27) and (B20) in (B19) and matching

like orders in J, we obtain

$$\hat{h}_0|n_{\rm o}, n_{\rm e}\rangle = e^{(0)}_{n_{\rm o}n_{\rm e}}|n_{\rm o}, n_{\rm e}\rangle, \tag{B28a}$$

$$\hat{h}_0|\psi^{(1)}_{n_{\rm o}n_{\rm e}}\rangle + \hat{h}|n_{\rm o}, n_{\rm e}\rangle = e^{(0)}_{n_{\rm o}n_{\rm e}}|\psi^{(1)}_{n_{\rm o}n_{\rm e}}\rangle + e^{(1)}_{n_{\rm o}n_{\rm e}}|n_{\rm o}, n_{\rm e}\rangle, \tag{B28b}$$

$$\hat{h}_0|\psi^{(2)}_{n_{\rm o}n_{\rm e}}\rangle + \hat{h}|\psi^{(1)}_{n_{\rm o}n_{\rm e}}\rangle + \hat{v}|n_{\rm o}, n_{\rm e}\rangle = e^{(0)}_{n_{\rm o}n_{\rm e}}|\psi^{(2)}_{n_{\rm o}n_{\rm e}}\rangle + e^{(1)}_{n_{\rm o}n_{\rm e}}|\psi^{(1)}_{n_{\rm o}n_{\rm e}}\rangle$$
$$+ e^{(2)}_{n_{\rm o}n_{\rm e}}|n_{\rm o}, n_{\rm e}\rangle, \tag{B28c}$$

etc. The first identity is just the unperturbed eigenproblem. On the other hand, projecting (B28b) onto $|n_{\rm o}, n_{\rm e}\rangle$ and using $\hat{a}_j|n_j\rangle = \sqrt{n_j}|n_j - 1\rangle$ and $\hat{a}_j^\dagger|n_j\rangle = \sqrt{n_j + 1}|n_j + 1\rangle$, we obtain the first-order correction to the eigenenergies,

$$e^{(1)}_{n_{\rm o}n_{\rm e}} = \langle n_{\rm o}, n_{\rm e}|\hat{h}|n_{\rm o}, n_{\rm e}\rangle = 2(\phi_{\rm o}^*\phi_{\rm e} - \phi_{\rm e}^*\phi_{\rm o}), \tag{B29}$$

while projecting (B28b) onto $|m_{\rm o} \neq n_{\rm o}, m_{\rm e} \neq n_{\rm e}\rangle$, we find the first-order corrections to the eigenvectors,

$$\langle m_{\rm o}, m_{\rm e}|\psi^{(1)}_{n_{\rm o}n_{\rm e}}\rangle = \frac{h_{m_{\rm o}m_{\rm e},n_{\rm o}n_{\rm e}}}{e^{(0)}_{n_{\rm o}n_{\rm e}} - e^{(0)}_{m_{\rm o}m_{\rm e}}}, \tag{B30}$$

with

$$\begin{aligned}
h_{m_{\rm o}m_{\rm e},n_{\rm o}n_{\rm e}} &= \langle m_{\rm o}, m_{\rm e}|\hat{h}|n_{\rm o}, n_{\rm e}\rangle \\
&= -2(\sqrt{n_{\rm o}}\phi_{\rm e}^*\delta_{m_{\rm o},n_{\rm o}-1}\delta_{m_{\rm e},n_{\rm e}} \\
&\quad + \sqrt{n_{\rm o}+1}\phi_{\rm e}\delta_{m_{\rm o},n_{\rm o}+1}\delta_{m_{\rm e},n_{\rm e}} \\
&\quad + \sqrt{n_{\rm e}}\phi_{\rm o}^*\delta_{m_{\rm o},n_{\rm o}}\delta_{m_{\rm e},n_{\rm e}-1} \\
&\quad + \sqrt{n_{\rm e}+1}\phi_{\rm o}\delta_{m_{\rm o},n_{\rm o}}\delta_{m_{\rm e},n_{\rm e}+1}).
\end{aligned} \tag{B31}$$

Finally, the second-order correction to the eigenenergies is found by projecting (B28c) onto $|n_{\rm o}, n_{\rm e}\rangle$, leading to

$$\begin{aligned}
e^{(2)}_{n_{\rm o}n_{\rm e}} &= \langle n_{\rm o}, n_{\rm e}|\hat{h}|\psi^{(1)}_{n_{\rm o}n_{\rm e}}\rangle + \langle n_{\rm o}, n_{\rm e}|\hat{v}|n_{\rm o}, n_{\rm e}\rangle \\
&= \sum_{m_{\rm o}\neq n_{\rm o}}\sum_{m_{\rm e}\neq n_{\rm e}}\frac{|h_{m_{\rm o}m_{\rm e},n_{\rm o}n_{\rm e}}|^2}{e^{(0)}_{n_{\rm o}n_{\rm e}} - e^{(0)}_{m_{\rm o}m_{\rm e}}},
\end{aligned} \tag{B32}$$

where we have used

$$\langle n_{\rm o}, n_{\rm e}|\hat{v}|n_{\rm o}, n_{\rm e}\rangle \sim \langle n_{\rm o}, n_{\rm e}|(\hat{n}_i - \hat{n}_j)|n_{\rm o}, n_{\rm e}\rangle = 0, \tag{B33a}$$

$$\begin{aligned}
\langle n_{\rm o}, n_{\rm e}|\hat{h}|\psi^{(1)}_{n_{\rm o}n_{\rm e}}\rangle &= \sum_{m_{\rm o}\neq n_{\rm o}}\sum_{m_{\rm e}\neq n_{\rm e}}\frac{h_{m_{\rm o}m_{\rm e},n_{\rm o}n_{\rm e}}}{e^{(0)}_{n_{\rm o}n_{\rm e}} - e^{(0)}_{m_{\rm o}m_{\rm e}}} \\
&\quad \times \underbrace{\langle n_{\rm o}, n_{\rm e}|\hat{h}|m_{\rm o}, m_{\rm e}\rangle}_{h^*_{m_{\rm o}m_{\rm e},n_{\rm o}n_{\rm e}}}.
\end{aligned} \tag{B33b}$$

Recombining the eigenenergies up to order J^2 as in (B20b) and particularizing to the ground state ($n_{\rm o} = \bar{n}_{\rm o}, n_{\rm e} = \bar{n}_{\rm e}$), we obtain the perturbative expression (B6) that we wanted to prove.

APPENDIX C: NUMERICAL SEARCH OF COHERENT-STATE MINIMA

In Sec. V we introduced the homogeneous and staggered coherent-state ansatz solutions that admitted a fully analytic treatment. One can ask whether there exist other solutions with an even lower energy. We have performed an exhaustive numerical search, finding many local minima, but never with energies below $E_{\rm SF}$ or $E_{\rm SS}$ of Eqs. (16) and (21), respectively.

In this Appendix we present the way in which we have performed the numerical search.

We have relied on imaginary-time evolution. In particular, we know that the energy of the state

$$|\psi(\tau)\rangle = \frac{e^{-\hat{H}\tau}|\psi(0)\rangle}{\langle\psi(0)|e^{-2\hat{H}\tau}|\psi(0)\rangle} \tag{C1}$$

should converge at $\tau \to \infty$ to that of the system's ground state, assuming that $|\psi(0)\rangle$ projects onto the ground subspace. The differential form of (C1) is

$$\partial_\tau|\psi(\tau)\rangle = -[\hat{H} - \langle\psi(\tau)|\hat{H}|\psi(\tau)\rangle]|\psi(\tau)\rangle, \tag{C2}$$

which has the form of a (nonlinear) Schrödinger equation where time has been replaced by an imaginary time $-i\tau$. We can particularize this equation to the coherent-state manifold by considering the ansatz of Sec. V,

$$|\psi(\tau)\rangle = \bigotimes_{j=1}^{L}|\alpha_j(\tau)\rangle, \tag{C3}$$

but now with τ-dependent coherent amplitudes $\alpha_j(\tau)$. We can then turn (C2) into an evolution or flow equation for these amplitudes by considering

$$\begin{aligned}
&\partial_\tau\langle\psi(\tau)|\hat{a}_j|\psi(\tau)\rangle \\
&= [\partial_\tau\langle\psi(\tau)|]\hat{a}_j|\psi(\tau)\rangle + \langle\psi(\tau)|\hat{a}_j[\partial_\tau|\psi(\tau)\rangle] \\
&= -\langle\psi(\tau)|(\hat{H}\hat{a}_j + \hat{a}_j\hat{H})|\psi(\tau)\rangle \\
&\quad + 2\langle\psi(\tau)|\hat{H}|\psi(\tau)\rangle\langle\psi(\tau)|\hat{a}_j|\psi(\tau)\rangle \\
&= -\langle\psi(\tau)|[\hat{a}_j, \hat{H}]|\psi(\tau)\rangle \\
&\quad + 2[\langle\psi(\tau)|\hat{H}\underbrace{\hat{a}_j|\psi(\tau)\rangle}_{\alpha_j|\psi(\tau)\rangle} - \langle\psi(\tau)|\hat{H}|\psi(\tau)\rangle \\
&\quad \times \underbrace{\langle\psi(\tau)|\hat{a}_j|\psi(\tau)\rangle}_{\alpha_j}]
\end{aligned} \tag{C4}$$

so that (here the overdot denotes derivative with respect to τ)

$$\begin{aligned}
\dot{\alpha}_j &= -\langle[\hat{a}_j, \hat{H}]\rangle = [\mu - U|\alpha_j|^2 + V(|\alpha_{j+1}|^2 + |\alpha_{j-1}|^2)]\alpha_j \\
&\quad + \varepsilon\alpha_j^* + J(\alpha_{j+1} + \alpha_{j-1}),
\end{aligned} \tag{C5}$$

where, after performing the commutator, we have used

$$\begin{aligned}
&\langle\hat{a}_{j_1}^\dagger\hat{a}_{j_2}^\dagger\cdots\hat{a}_{j_J}^\dagger\hat{a}_{j_{J+1}}\hat{a}_{j_{J+2}}\cdots\hat{a}_{j_{J+K}}\rangle \\
&= \alpha_{j_1}^*\alpha_{j_2}^*\cdots\alpha_{j_J}^*\alpha_{j_{J+1}}\alpha_{j_{J+2}}\cdots\alpha_{j_{J+K}}
\end{aligned} \tag{C6}$$

for the normally ordered product of J creation operators with K annihilation operators in a coherent state. From any initial configuration $\{\alpha_j(0)\}_{j=1,2,\ldots,L}$ (different from a fixed point), this nonlinear system will deterministically flow towards one of its attractors, corresponding to a local (or global) minimum of the energy functional of Eq. (13). We have tried a huge number of random initial configurations for sizes L as large as a few hundreds, always flowing into either the analytical solutions presented in the previous Appendixes or other configurations with higher energy.

APPENDIX D: GENERAL GAUSSIAN-STATE ANSATZ

In order to confirm the predictions from the coherent-state ansatz, we have extended the variational space by considering all possible Gaussian states. We will show that the predictions from this general ansatz converge to the analytical ones obtained in Appendix C as we move deeper into the region with Z_2-superfluid order.

Gaussian states refer to those with a Gaussian Wigner function [44,84–87] such that their statistics are completely characterized by first- and second-order moments. Let us define the position and momentum quadratures $\hat{x}_j = \hat{a}_j^\dagger + \hat{a}_j$ and $\hat{p}_j = i(\hat{a}_j^\dagger - \hat{a}_j)$, which we collect in the column vector $\hat{\boldsymbol{r}} = (\hat{x}_1, \ldots, \hat{x}_L, \hat{p}_1, \ldots, \hat{p}_L)^\mathsf{T}$, where T transposes the array without altering the operators that form it. Note that the canonical commutation relations read

$$[\hat{r}_m, \hat{r}_n] = 2i\Omega_{mn}, \quad \text{with} \quad \Omega = \begin{pmatrix} 0 & \mathcal{I} \\ -\mathcal{I} & 0 \end{pmatrix}, \quad \text{(D1)}$$

with $\mathcal{I}$ the $L \times L$ identity matrix and Ω known as the symplectic form. First- and second-order moments are characterized by the mean vector $d_m = \langle \hat{r}_m \rangle$ and the covariance matrix $V_{mn} = \langle \delta\hat{r}_m \delta\hat{r}_n + \delta\hat{r}_n \delta\hat{r}_m \rangle / 2$, respectively, where we have defined the quadrature fluctuations $\delta\hat{r}_m = \hat{r}_m - d_m$. In a more compact notation

$$\boldsymbol{d} = \langle \hat{\boldsymbol{r}} \rangle \in \mathbb{R}^{2L}, \quad \text{(D2a)}$$

$$V = \langle \delta\hat{\boldsymbol{r}} \delta\hat{\boldsymbol{r}}^\mathsf{T} \rangle - i\Omega \in \mathbb{R}^{2L} \times \mathbb{R}^{2L}, \quad \text{(D2b)}$$

where we have used the commutation relations (4) in (D2b). Higher-order moments can be found from first- and second-order ones via the Gaussian moment theorem [44,88]. Consider a set of K operators $\{\hat{L}_k\}_{k=1,2,\ldots,K}$, all arbitrary linear functions of the quadrature fluctuations; this theorem states that

$$\langle \hat{L}_1 \hat{L}_2 \cdots \hat{L}_K \rangle = \begin{cases} 0 & \text{for odd } K \\ \sum_{\substack{\{k_1,k_2,\ldots,k_K\} \in \\ (K-1)!! \text{ pairings}}} \langle \hat{L}_{k_1} \hat{L}_{k_2} \rangle \cdots \langle \hat{L}_{k_{K-1}} \hat{L}_{k_K} \rangle & \text{for even } K. \end{cases} \quad \text{(D3)}$$

Together with the relation $\langle \delta\hat{r}_m \delta\hat{r}_n \rangle = V_{mn} + i\Omega_{mn}$, this allows connecting the expectation value of any polynomial function of the quadratures to a polynomial of the elements of the mean vector and covariance matrix of the Gaussian state. Crucially, since the Hamiltonian (1) is a fourth-order polynomial in the annihilation and creation operators (or the quadratures, since $2\hat{a}_j = \hat{x}_j + i\hat{p}_j$), the energy functional $E(\boldsymbol{d}, V) = \langle \hat{H} \rangle$ can be found as a function of the mean vector and covariance matrix by using this Gaussian moment theorem (D3). While this can be a tedious task, it is conceptually simple. The Binder parameter as defined in the main text is determined from the ratio between eighth-order polynomials in the quadratures and it is another quantity that we will use extensively in this Appendix, which we compute via the Gaussian moment theorem.

It is not difficult to prove [44,84–87] that any pure Gaussian state $|\psi(V, \boldsymbol{d})\rangle$ characterized by its mean vector and covariance matrix can be generated by applying some Gaussian unitary $\hat{G}$ onto the vacuum state

$$|\psi(V, \boldsymbol{d})\rangle = \hat{G}|\text{vac}\rangle, \quad \text{with} \quad \hat{a}_j|\text{vac}\rangle = 0, \quad \text{(D4)}$$

where Gaussian unitaries are defined as those that perform a linear transformation on the quadratures

$$\hat{G}^\dagger \hat{\boldsymbol{r}} \hat{G} = S\hat{\boldsymbol{r}} + \boldsymbol{d}. \quad \text{(D5)}$$

Preservation of the canonical commutation relations imposes that the matrix S is constrained to the special symplectic group of L modes, $\text{Sp}(2L, \mathbb{R})$, that is, it has unit determinant and must leave invariant the symplectic form Ω,

$$S\Omega S^\mathsf{T} = \Omega. \quad \text{(D6)}$$

Taking into account that the covariance matrix of vacuum is the $2L \times 2L$ identity, Eqs. (D2), (D4), and (D5) imply the relation

$$V = SS^\mathsf{T} \quad \text{(D7)}$$

between the covariance matrix of the Gaussian state and the Gaussian unitary that defines it. The coherent states of Appendix C, Eq. (C3), correspond to Gaussian states with V equal to the identity $d_j = 2\,\text{Re}(\alpha_j)$ and $d_{L+j} = 2\,\text{Im}(\alpha_j)$.

In order to find the ground state within the Gaussian variational manifold we make use again of imaginary-time evolution. Considering a Gaussian state with τ-dependent variational parameters $\boldsymbol{d}(\tau)$ and $V(\tau)$, it is possible to show [89] using (D4) that the imaginary-time Schrödinger equation (C2) is transformed into

$$\dot{\boldsymbol{d}} = -2V\boldsymbol{u}(\boldsymbol{d}, V), \quad \text{(D8a)}$$

$$\dot{V} = 4\Omega^T \mathcal{M}(\boldsymbol{d}, V)\Omega - 4V\mathcal{M}(\boldsymbol{d}, V)V, \quad \text{(D8b)}$$

where we have defined a vector and a matrix containing the derivatives of the energy functional with respect the variational parameters

$$u_m = \frac{\partial E}{\partial d_m}, \quad \text{(D9a)}$$

$$\mathcal{M}_{mn} = \frac{\partial E}{\partial V_{mn}}. \quad \text{(D9b)}$$

For a given parameter set, we simulate these flow equations (D8) starting from many random mean vectors and covariance matrices, up to a sufficiently long time τ that ensures convergence to a fixed point of the equations (corresponding, as in the coherent case, to a local minimum of the energy landscape). We then select the one providing the lowest energy.

Before presenting the results, let us comment on one subtle point related to how we generate random (but physical) covariance matrices. We exploit the Bloch-Messiah reduction or Euler decomposition of symplectic matrices [84,85,87] so that
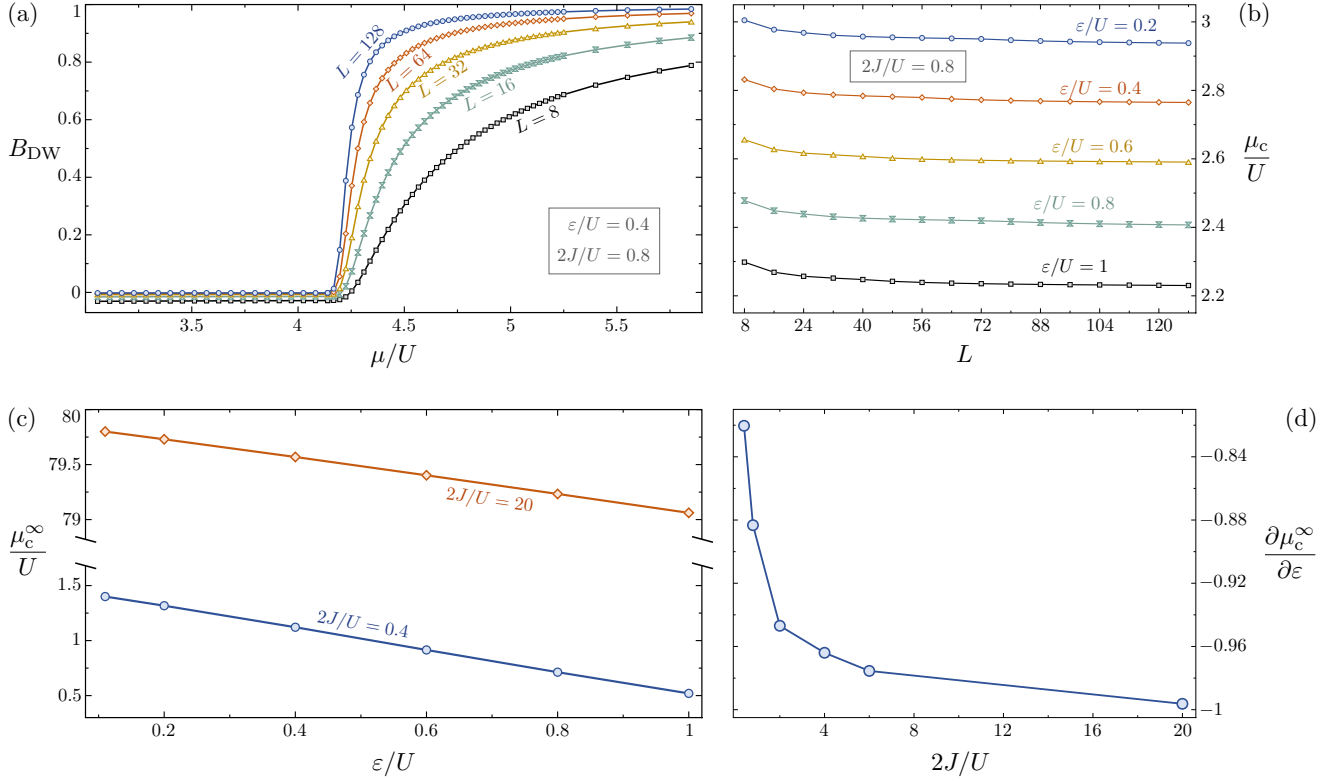
FIG. 7. Results from the general Gaussian ground-state ansatz for $2V/U = 1.5$. (a) Binder parameter B as a function of μ/U for increasing system sizes L. The values $2J/U = 0.8$ and $\varepsilon/U = 0.4$ have been chosen for this plot, but similar plots emerge for other values. It is evident that a transition from homogeneous to staggered superfluid (Z_2-SF to Z_2-SS) is predicted at some critical chemical potential. (b) Largest value of the chemical potential for which the Binder parameter is zero, which we define as μ_c/U, as a function of the system size L, for different values of ε/U and $2J/U = 0.8$. It is clear that μ_c/U converges towards some value μ_c^∞/U as L increases. In (c) we plot this value as a function of ε/U for two values of $2J/U$. We can appreciate a linear relationship that is also found for any other value of $2J/U$. Finally, in (d) we plot the slope of the previous straight lines, $\partial\mu_c^\infty/\partial\varepsilon$, for different values of $2J/U$. The slope tends to -1 as $2J/U$ increases, confirming the coherent-state prediction $\mu_c \sim -\varepsilon$.

Eq. (D7) allows us to sample covariance matrices as

$$V = K^{\mathrm{T}}DK, \tag{D10}$$

where $D = \mathrm{diag}(e^{-2r_1}, \ldots, e^{-2r_L}, e^{2r_1}, \ldots, e^{2r_L})$ is a diagonal matrix with real and positive random numbers r_j (technically D is the covariance matrix of L independent squeezed vacuum states [44,84–87]) and K is a symplectic orthogonal matrix (so-called interferometer) that can be built as [87]

$$K = \begin{pmatrix} X & -Y \\ Y & X \end{pmatrix}, \tag{D11}$$

with X and Y the real and imaginary parts of a random $L \times L$ unitary matrix $Q = X + iY$ that we can generate from the QR decomposition of any random complex matrix.

Our results are summarized in Fig. 7. Our goal is showing that the general Gaussian ansatz is compatible with the coherent-state ansatz deep in the superfluid region. In particular, we aim at showing that there is an asymptotic $\mu \sim -\varepsilon$ relation between the chemical potential and the pair injection at the critical boundary separating the SF and SS phases as $2J/U$ increases. To this aim, we proceed as follows. We set $2V/U = 1.5$. Then, for any value of $2J/U$ and ε/U we expect a transition from SF to SS for some value of μ/U. We

use the Binder parameter to perform a finite-size scaling and determine the critical μ/U as a function of ε/U for different values of J/U. An example of the behavior of this parameter is shown in Fig. 7(a) for $J/U = 0.4 = \varepsilon/U$ (similar figures are found for any other values). We check system sizes ranging from $L = 8$ to 128, as specified in the figure. For all of them, the Binder parameter changes from zero (or right below zero) to a positive increasing function closer to a step function the larger L is. For a given system size L, we then define the critical chemical potential μ_c as the largest μ for which B is zero (we estimate it by interpolating the points via the Makima algorithm, consisting of piecewise third-order polynomials with continuous first-order derivatives). In Fig. 7(b) we show this μ_c as a function of L (for different values of ε and $J = 0.4$), which is expected to adhere to a power law of the type $\mu_c = \mu_c^\infty + \beta L^{-\eta}$ for some positive parameters $\{\mu_c^\infty, \beta, \eta\}$. Indeed, we find that such a curve fits nicely to our data, allowing us to estimate the critical chemical potential μ_c^∞/U and find a nice linear dependence on ε/U [Fig. 7(c)] for each value of J/U. Finally, we consider the slope $\partial\mu_c^\infty/\partial\varepsilon$ of those linear curves as a function of J/U, finding that it approaches -1 as J/U increases, that is, as we move deeper into the superfluid region. This serves as support for the coherent-state predictions.

APPENDIX E: UNBALANCED COHERENT-STATE ANSATZ SOLUTIONS FOR THE MODEL WITH U(1) SYMMETRY

In Sec. VI we studied an extension of the original model (1) with U(1) symmetry and two modes per site. Within a coherent-state ansatz, we explained that the model had balanced solutions with equal amplitudes for both local modes, as well as unbalanced solutions, for which the amplitudes of the local modes differ. The balanced subspace followed the exact same results that we already found for the original Hamiltonian (1). In this Appendix we discuss how we have concluded that this is the relevant subspace, since the minima of the unbalanced subspace have larger energy in all parameter space.

It is easy to prove that homogeneous unbalanced solutions to Eq. (25) exist only when $2\varepsilon \leqslant \mu + 2J$, with

$$2\alpha_j^2 = \mu + 2J \pm \sqrt{(\mu + 2J)^2 - 4\varepsilon^2} \ \forall \ j, \qquad \text{(E1a)}$$

$$2\beta_j^2 = \mu + 2J \mp \sqrt{(\mu + 2J)^2 - 4\varepsilon^2} \ \forall \ j. \qquad \text{(E1b)}$$

These have an energy $E = -L[3\varepsilon^2 + (\mu + 2J)^2/2]/(U + 2V)$, which is easily proven to be larger than that of the balanced homogeneous solutions, corresponding to twice that in Eq. (16). It is also easy (but lengthy) to find staggered unbalanced solutions semianalytically, but these are also shown to have larger energy than the balanced solutions in the region of parameters that we have discussed in this work. The same conclusion is drawn from the exhaustive search that we have carried by numerically simulating the imaginary-time dynamical equations equivalent to those derived in Appendix C for the previous model starting from random initial conditions,

$$\dot{\alpha}_j = -\langle[\hat{a}_j, \hat{H}]\rangle = [\mu - U|\alpha_j|^2 + V(|\alpha_{j+1}|^2 + |\alpha_{j-1}|^2)]\alpha_j$$
$$+ \varepsilon\beta_j^* + J(\alpha_{j+1} + \alpha_{j-1}), \qquad \text{(E2a)}$$

$$\dot{\beta}_j = -\langle[\hat{b}_j, \hat{H}]\rangle = [\mu - U|\beta_j|^2 + V(|\beta_{j+1}|^2 + |\beta_{j-1}|^2)]\beta_j$$
$$+ \varepsilon\alpha_j^* + J(\beta_{j+1} + \beta_{j-1}). \qquad \text{(E2b)}$$

APPENDIX F: DERIVATION OF THE MASTER EQUATION

Here we explain how the master equation (27) is obtained as a model that closely describes how pair injection is implemented experimentally. While the specifics of the environment and its coupling to the system might differ on each experimental platform, we can use a generic model that has the essential ingredients that are found on all platforms. To ease the notation, let us simplify the system to a single bosonic mode with annihilation operator $\hat{a}$ and energy ω_0 (the generalization to the full bosonic array will be easily carried out later). We consider an environment consisting of a continuous set of bosonic modes with annihilation operators $\hat{b}(\omega)$, labeled by their characteristic frequency ω, satisfying canonical commutation relations $[\hat{b}(\omega), \hat{b}(\omega')] = 0$ and $[\hat{b}(\omega), \hat{b}^\dagger(\omega')] = \delta(\omega - \omega')$ [44]. As specific examples, for an optical cavity this environment models the external field in empty space [90,91]; for a superconducting circuit, it might be the microwave field propagating in a transmission line or the modes of a lossy circuit [32]; for cold atoms trapped in optical lattices, it might correspond to the same atoms in another internal state [61–63,92,93] or to diatomic molecules [64–66]

trapped in a shallow potential. The Hamiltonian describing the whole system plus environment is given by

$$\hat{H}_{s+e} = \underbrace{\omega_0\hat{a}^\dagger\hat{a}}_{\hat{H}_{sys}} + \underbrace{\int_{\omega\in O(2\omega_0)} d\omega\,\omega\hat{b}^\dagger(\omega)\hat{b}(\omega)}_{\hat{H}_{env}}$$
$$+ \underbrace{\int_{\omega\in O(2\omega_0)} d\omega\sqrt{g(\omega)}[\hat{a}^{\dagger 2}\hat{b}(\omega) + \hat{a}^2\hat{b}^\dagger(\omega)]}_{\hat{H}_{int}}, \quad \text{(F1)}$$

where we have included a coupling between the system's mode and each environmental mode with strength $g(\omega) \ll \omega_0$ (note that the square root is added in the definition of the interaction so that g has units of energy). Any interaction aimed at implementing pair injection needs to exchange environmental excitations with pairs of system excitations, a process that is only efficient for environmental modes with energies ω around $2\omega_0$. We emphasize this by limiting the integration domain to $O(2\omega_0)$, understood as frequencies around $2\omega_0$ within a bandwidth proportional to the energy g provided by the interaction. Of course, linear coupling to environmental degrees of freedom around frequencies ω_0 will most likely exist as well in experiments, say, a term

$$\int_{\omega\in O(\omega_0)} d\omega\sqrt{g(\omega)}[\hat{a}^\dagger\hat{b}(\omega) + \hat{a}\hat{b}^\dagger(\omega)]. \qquad \text{(F2)}$$

As we note at the end of this Appendix, this would induce conventional linear damping in the system. We focus here on the quadratic coupling of (F1) because it is the one we use to drive the system, ultimately generating coherent pair injection.

The way in which the interaction (F1) is accomplished between the system and the environment varies from platform to platform. Photonic systems systems are the neatest one, since this interaction naturally occurs inside materials with a second-order nonlinear polarization response to the electric field [44,71,90,94] so the electromagnetic energy inside them (the polarization field times the electric field) contains a term cubic in the field, ultimately leading precisely to (F1). In this context, such an interaction is referred to as down-conversion or three-wave mixing with more generality, since one excitation of the environment is converted into two excitations of the system and vice versa, involving three waves in the process. In other platforms the coupling between the system and the environment takes a four-wave-mixing form of the type $\hat{b}_+(\omega)\hat{b}_-(\omega)\hat{a}^{\dagger 2} + \text{H.c.}$, where now the environment has two modes per frequency, which satisfy canonical commutation relations $[\hat{b}_\sigma(\omega), \hat{b}_{\sigma'}^\dagger(\omega')] = \delta_{\sigma\sigma'}\delta(\omega - \omega')$ and $[\hat{b}_\sigma(\omega), \hat{b}_{\sigma'}(\omega')] = 0$. In superconducting circuits [32–34,37–40] this interaction emerges when the coupling between the system's mode at frequency ω_0 and two environmental modes close to the sidebands $\omega_0 \pm \Delta\omega$ (with $\Delta\omega \gg g$) occurs through a Josephson junction, whose stored energy has a quartic response to the flux crossing it. In cold atoms [61–63], this quartic interaction comes about when, for example, the atoms trapped in the optical lattice have a hyperfine magnetic number 0, while the environmental atoms moving in a shallow trap have hyperfine magnetic numbers ± 1, so conservation of angular momentum forces s-wave scattering to have the

quartic form introduced above. From the theoretical point of view, this quartic system-environment interaction just complicates slightly the technical derivation that we present below, but without adding any conceptual difference. Hence we stick with the form (F1) to illustrate how the master equation (27) comes about.

Before integrating out the environment, we need to discuss its state in the absence of coupling to the system. Here is where the word "driving" gains a definition: This usually refers to the fact that a coherent state is generated in the environment, for example, by making it correspond to the output of a laser or a microwave generator in optical systems or superconducting circuits, respectively, or to a Bose-Einstein condensate in cold atoms. Coherent states are the most classical (pure) states one can build in quantum field theory, essentially leading, when used as an ansatz, to classical field theory onto which vacuum fluctuations are superimposed. Such coherent states are characterized by the complex amplitude $\langle \hat{b}(\omega) \rangle \equiv \beta(\omega) e^{-i\omega t}$ that they produce on the environmental modes, where $|\beta(\omega)|^2 d\omega$ is the number of excitations present in the infinitesimal interval $[\omega, \omega + d\omega]$. As Hilbert space vectors, these coherent environmental states are written as the functional [44]

$$|\psi_{\text{env}}[\beta](t)\rangle = \underbrace{\exp\left(\int_{\omega \in O(2\omega_0)} d\omega [\beta(\omega) e^{-i\omega t} \hat{b}^\dagger(\omega) - \beta^*(\omega) e^{i\omega t} \hat{b}(\omega)]\right)}_{\hat{D}(t)} |\text{vac}\rangle, \tag{F3}$$

where we have defined the environmental vacuum state that satisfies $\hat{b}(\omega)|\text{vac}\rangle = 0$ and the so-called displacement operator $\hat{D}(t)$. It is not difficult to see that these states satisfy the environmental Schrödinger equation $i\partial_t |\psi_{\text{env}}\rangle = \hat{H}_{\text{env}}|\psi_{\text{env}}\rangle$ [44]. For our purposes, we choose $\beta(\omega) = -\beta_{\text{d}}\delta(\omega - 2\omega_{\text{d}})$, which corresponds to an environment that drives the system monochromatically at frequency $2\omega_{\text{d}}$, as we will shortly see explicitly (the factor 2 in the driving frequency and the negative driving amplitude are chosen for later convenience). In the following we take β_{d} real and positive for definiteness.

In order to integrate out the environmental degrees of freedom, it is more convenient to work in a picture where the environment is in the vacuum state. Denoting by $\hat{\rho}^{(s+e)}(t)$ the state of the system plus environment in the Schrödinger picture, we then work in a new picture where the displacement (F3) is removed. To this aim, we define a new state $\hat{\rho}_D^{(s+e)} = \hat{D}^\dagger(t)\hat{\rho}^{(s+e)}(t)\hat{D}(t)$ that evolves according to the Hamiltonian [44]

$$\hat{H}_D(t) = \hat{D}^\dagger(t)\hat{H}_{s+e}\hat{D}(t) - i\hat{D}^\dagger(t)\partial_t \hat{D}(t)$$
$$= \hat{H}_{\text{sys}} \underbrace{-\sqrt{g(\omega_{\text{d}})}\beta_{\text{d}}(e^{-2i\omega_{\text{d}}t}\hat{a}^{\dagger 2} + e^{2i\omega_{\text{d}}t}\hat{a}^2)}_{\hat{H}_{\text{d}}(t)} + \hat{H}_{\text{env}}$$
$$+ \hat{H}_{\text{int}}, \tag{F4}$$

where we have used

$$\hat{D}^\dagger(t)\hat{b}(\omega)\hat{D}(t) = \hat{b}(\omega) + \beta(\omega)e^{-i\omega t}, \tag{F5a}$$

$$i\partial_t \hat{D}(t) = \hat{D}(t)\left[\int_{-\infty}^{+\infty} d\omega \beta(\omega)\omega e^{-i\omega t} \right.$$
$$\left. \times \left(\hat{b}^\dagger(\omega) + \frac{\beta^*(\omega)e^{i\omega t}}{2}\right) - \text{H.c.}\right]. \tag{F5b}$$

This picture deals with a simplified environmental state (vacuum) at the expense of working with a more complicated system Hamiltonian $\hat{H}'_{\text{sys}}(t) = \hat{H}_{\text{sys}} + \hat{H}_{\text{d}}(t)$ but leaving the environmental Hamiltonian $\hat{H}_{\text{env}}$ and the interaction $\hat{H}_{\text{int}}$ untouched.

Since we are about to use perturbation theory as a last step, the integration of the environmental degrees of freedom is better performed in the interaction picture. This is defined by discounting all dynamics but the one generated by $\hat{H}_{\text{int}}$. We then define the unitary operator ($\mathcal{T}$ is the time-ordering symbol [44])

$$\hat{U}(t) = \mathcal{T}\left[\exp\left(-i\int_0^t dt' \hat{H}'_{\text{sys}}(t')\right)\right]e^{-i\hat{H}_{\text{env}}t}, \tag{F6}$$

which transforms the environmental operators as

$$\hat{U}^\dagger(t)\hat{b}(\omega)\hat{U}(t) = e^{-i\omega t}\hat{b}(\omega). \tag{F7}$$

The transformed state $\hat{\rho}_I^{(s+e)} = \hat{U}^\dagger(t)\hat{\rho}_D^{(s+e)}\hat{U}(t)$ evolves then according to the von Neumann equation

$$i\partial_t \hat{\rho}_I^{(s+e)} = [\hat{H}_I(t), \hat{\rho}_I^{(s+e)}], \tag{F8}$$

with an interaction-picture Hamiltonian

$$\hat{H}_I(t) = \hat{U}^\dagger(t)\underbrace{[\hat{H}_D(t) - \hat{H}'_{\text{sys}}(t) - \hat{H}_{\text{env}}]}_{\hat{H}_{\text{int}}}\hat{U}(t) \tag{F9}$$

$$= \int_{\omega \in O(2\omega_0)} d\omega \sqrt{g(\omega)}\left[e^{-i\omega t}\hat{a}_I^{\dagger 2}(t)\hat{b}(\omega)\right.$$
$$\left. + e^{i\omega t}\hat{a}_I^2(t)\hat{b}^\dagger(\omega)\right],$$

where we have defined the interaction-picture system operators $\hat{a}_I(t) = \hat{U}^\dagger(t)\hat{a}\hat{U}(t)$.

We now find an evolution equation for the reduced state of the system $\hat{\rho}_I = \text{tr}_{\text{env}}(\hat{\rho}_I^{(s+e)})$, by keeping effects on its dynamics up to second order in the interaction. To this aim, let us first consider the integral form of the von Neumann equation (F8)

$$\hat{\rho}_I^{(s+e)}(t) = \hat{\rho}_I(0) \otimes |\text{vac}\rangle\langle\text{vac}| - i\int_0^t dt'[\hat{H}_I(t'), \hat{\rho}_I^{(s+e)}(t')], \tag{F10}$$

where we have assumed that the system and the environment start in an uncorrelated state. Reinserting this on the right-hand side of (F8) and performing the partial trace over the environmental modes, we obtain

$$\partial_t \hat{\rho}_I(t) = -\int_0^t d\tau \, \text{tr}_{\text{env}}\{[\hat{H}_I(t), [\hat{H}_I(t-\tau), \hat{\rho}_I^{(s+e)}(t-\tau)]]\}, \tag{F11}$$

where we have used $\langle\text{vac}|\hat{H}_{\text{I}}|\text{vac}\rangle = 0$ and made the integration variable change $\tau = t - t'$ for later convenience. This equation is explicitly second order on the interaction. Hence, if we want to stay at that order of approximation, we can neglect all effects on $\hat{\rho}_{\text{I}}^{(\text{s+e})}(t - \tau)$ beyond trivial order. This is known as the Born-Markov approximation. The Born approximation can be seen as a combination of two approximations: First, the correlations between the system and the environment are neglected; then the backaction of the system onto the (comparatively larger) environment is neglected [44,69,70]. Hence, within the Born approximation, the state on the right-hand side is approximated by $\hat{\rho}_{\text{I}}^{(\text{s+e})}(t - \tau) = \hat{\rho}_{\text{I}}(t - \tau) \otimes |\text{vac}\rangle\langle\text{vac}|$, which allows performing the environmental trace explicitly, obtaining

$$\partial_t \hat{\rho}_{\text{I}}(t) = \int_0^t d\tau\, C(\tau)\big[\hat{a}_{\text{I}}^2(t)\hat{\rho}_{\text{I}}(t - \tau)\hat{a}_{\text{I}}^{\dagger 2}(t - \tau)$$
$$- \hat{\rho}_{\text{I}}(t - \tau)\hat{a}_{\text{I}}^{\dagger 2}(t - \tau)\hat{a}_{\text{I}}^2(t)\big] + \text{H.c.}, \quad \text{(F12)}$$

where we have defined the environmental correlation function $C(\tau) = \int_{\omega \in O(2\omega_0)} d\omega\, g(\omega)e^{i\omega\tau}$. In most common situations, the couplings $g(\omega)$ vary slowly with ω, so this is a function that decays quite fast with τ as we show shortly. One invokes then the Markov approximation [44,69,70], where it is assumed that this decay is much faster than any evolution rate of the system, so that we can set $\tau \to 0$ in the state $\hat{\rho}_{\text{I}}(t - \tau)$ and the bosonic operators $\hat{a}_{\text{I}}(t - \tau)$. In order to justify this assumption, let us recall that only frequencies around $2\omega_0$ contribute to the physics of the problem, so we should not make a big error by extending the integration domain to $\omega \in [-\infty, \infty]$ and setting the value of the couplings to $g(2\omega_0)\,\forall\,\omega$. This is sometimes called the strong Markov approximation and leads to $C(\tau) = 2\pi g(2\omega_0)\delta(\tau)$, that is, a correlation function that decays infinitely fast (infinite decay rate), allowing for contributions only at $\tau = 0$. Performing the Markov approximation (in its strong form for simplicity), we turn (F12) into

$$\partial_t \hat{\rho}_{\text{I}}(t) = g(2\omega_0)\pi\big[\hat{a}_{\text{I}}^2(t)\hat{\rho}_{\text{I}}(t)\hat{a}_{\text{I}}^{\dagger 2}(t)$$
$$- \hat{a}_{\text{I}}^{\dagger 2}(t)\hat{a}_{\text{I}}^2(t)\hat{\rho}_{\text{I}}(t) + \text{H.c.}\big]. \quad \text{(F13)}$$

Finally, returning to the original Schrödinger picture, the system's state $\hat{\rho}(t) = \hat{U}(t)\hat{\rho}_{\text{I}}(t)\hat{U}^\dagger(t)$ evolves according to the master equation

$$\partial_t \hat{\rho} = -i[\hat{H}(t), \hat{\rho}] + \gamma(2\hat{a}^2\hat{\rho}\hat{a}^{\dagger 2} - \hat{a}^{\dagger 2}\hat{a}^2\hat{\rho} - \hat{\rho}\hat{a}^{\dagger 2}\hat{a}^2),$$
$$\text{(F14)}$$

with the Hamiltonian

$$\hat{H}(t) = \omega_0\hat{a}^\dagger\hat{a} - \frac{\varepsilon}{2}(e^{-2i\omega_d t}\hat{a}^{\dagger 2} + e^{2i\omega_d t}\hat{a}^2), \quad \text{(F15)}$$

where we made the identifications $\varepsilon = \beta_d g(2\omega_d)$ and $\gamma = \pi g(2\omega_0)$. Note that the Markov approximation requires that these parameters must be much smaller than the decay rate of the environmental correlator. This is a condition that one has to be careful to satisfy in experiments unless specifically looking for non-Markovian effects.

The master equation (F14) is the single-mode equivalent of the one we were set to derive, Eq. (27). The generalization to a bosonic array is straightforward, assuming that each mode of the array is connected to its own environment and that the extended Bose-Hubbard Hamiltonian (29) satisfies the Markov conditions (meaning that, in addition to ε and γ, the rest of parameters J, U, V, and μ are also much smaller than the decay rate of the environmental correlator).

Finally, let us comment on the effect that a linear coupling of the system to the environment of the type (F2) would have. Following the same procedure derived above for the quadratic coupling but simplified by the fact that the environment around frequency ω_0 is in the vacuum state, we would obtain an extra dissipative term in (F14) of the type $\kappa(2\hat{a}\hat{\rho}\hat{a}^\dagger - \hat{a}^\dagger\hat{a}\hat{\rho} - \hat{\rho}\hat{a}^\dagger\hat{a})$, with $\kappa = \pi g(\omega_0)$. This leads, when extended to all lattice sites, to the terms introduced in the master equation (27). Note that no linear coherent injection of the type $\varepsilon(e^{-i\omega_d t}\hat{a}^\dagger + e^{i\omega_d t}\hat{a})$ is added from this environment because we are not driving it, that is, all environmental modes with frequencies $\omega \in O(\omega_0)$ are in the vacuum state. Moreover, we find it important to remark that the environments with modes around frequencies $2\omega_0$ and ω_0 typically couple to the system through completely different physical mechanisms and hence γ and κ can be independently tuned. In other words, one should not see the coupling in (F1) as second-order term accompanying (F2) in a perturbative expansion, which would suggest $\gamma \ll \kappa$. In fact, experiments reporting $\gamma \gg \kappa$ have been carried in superconducting circuits [33].

[1] J. I. Cirac and P. Zoller, Nat. Phys. **8**, 264 (2012).

[2] I. Bloch, J. Dalibard, and S. Nascimbène, Nat. Phys. **8**, 267 (2012).

[3] R. Blatt and C. F. Roos, Nat. Phys. **8**, 277 (2012).

[4] A. Aspuru-Guzik and P. Walther, Nat. Phys. **8**, 285 (2012).

[5] A. A. Houck, H. E. Türeci, and J. Koch, Nat. Phys. **8**, 292 (2012).

[6] I. M. Georgescu, S. Ashhab, and F. Nori, Rev. Mod. Phys. **86**, 153 (2014).

[7] E. Altman, K. R. Brown, G. Carleo, L. D. Carr, E. Demler, C. Chin, B. DeMarco, S. E. Economou, M. A. Eriksson, K.-M. C. Fu, M. Greiner, K. R. A. Hazzard, R. G. Hulet, A. J. Kollár, B. L. Lev, M. D. Lukin, R. Ma, X. Mi, S. Misra, C. Monroe *et al.*, PRX Quantum **2**, 017003 (2021).

[8] D. P. Arovas, E. Berg, S. A. Kivelson, and S. Raghu, Annu. Rev. Condens. Matter Phys. **13**, 239 (2022).

[9] O. Dutta, M. Gajda, P. Hauke, M. Lewenstein, D.-S. Lühmann, B. A. Malomed, T. Sowiński, and J. Zakrzewski, Rep. Prog. Phys. **78**, 066001 (2015).

[10] M. Lewenstein, A. Sanpera, V. Ahufinger, B. Damski, A. Sen(De), and U. Sen, Adv. Phys. **56**, 243 (2007).

[11] M. P. A. Fisher, P. B. Weichman, G. Grinstein, and D. S. Fisher, Phys. Rev. B **40**, 546 (1989).

[12] J. Hubbard, Proc. R. Soc. London Ser. A **277**, 237 (1964).

[13] I. Bloch, J. Dalibard, and W. Zwerger, Rev. Mod. Phys. **80**, 885 (2008).

[14] D. Jaksch and P. Zoller, Ann. Phys. (NY) **315**, 52 (2005).

[15] I. Carusotto and C. Ciuti, Rev. Mod. Phys. **85**, 299 (2013).

[16] T. Ozawa, H. M. Price, A. Amo, N. Goldman, M. Hafezi, L. Lu, M. C. Rechtsman, D. Schuster, J. Simon, O. Zilberberg, and I. Carusotto, Rev. Mod. Phys. **91**, 015006 (2019).

[17] T. Boulier, M. J. Jacquet, A. Maître, G. Lerario, F. Claude, S. Pigeon, Q. Glorieux, A. Bramati, E. Giacobino, A. Amo, and J. Bloch, arXiv:2005.12569

[18] D. D. Solnyshkov, G. Malpuech, P. St-Jean, S. Ravets, J. Bloch, and A. Amo, Opt. Mater. Express **11**, 1119 (2021).

[19] J. Bloch, I. Carusotto, and M. Wouters, Nat. Rev. Phys. **4**, 470 (2022).

[20] O. Mansikkamäki, S. Laine, A. Piltonen, and M. Silveri, PRX Quantum **3**, 040314 (2022).

[21] O. Mansikkamäki, S. Laine, and M. Silveri, Phys. Rev. B **103**, L220202 (2021).

[22] A. Blais, A. L. Grimsmo, S. M. Girvin, and A. Wallraff, Rev. Mod. Phys. **93**, 025005 (2021).

[23] P. Krantz, M. Kjaergaard, F. Yan, T. P. Orlando, S. Gustavsson, and W. D. Oliver, Appl. Phys. Rev. **6**, 021318 (2019).

[24] X. Gu, A. F. Kockum, A. Miranowicz, Y.-x. Liu, and F. Nori, Phys. Rep. **718-719**, 1 (2017).

[25] M. Dalmonte, S. I. Mirzaei, P. R. Muppalla, D. Marcos, P. Zoller, and G. Kirchmair, Phys. Rev. B **92**, 174507 (2015).

[26] S. Schmidt and J. Koch, Ann. Phys. (Berlin) **525**, 395 (2013).

[27] A. Le Boité, G. Orso, and C. Ciuti, Phys. Rev. Lett. **110**, 233601 (2013).

[28] A. Le Boité, G. Orso, and C. Ciuti, Phys. Rev. A **90**, 063821 (2014).

[29] S. Hacohen-Gourgy, V. V. Ramasesh, C. De Grandi, I. Siddiqi, and S. M. Girvin, Phys. Rev. Lett. **115**, 240501 (2015).

[30] M. Fitzpatrick, N. M. Sundaresan, A. C. Y. Li, J. Koch, and A. A. Houck, Phys. Rev. X **7**, 011016 (2017).

[31] R. Ma, B. Saxberg, C. Owens, N. Leung, Y. Lu, J. Simon, and D. I. Schuster, Nature (London) **566**, 51 (2019).

[32] Z. Leghtas, S. Touzard, I. M. Pop, A. Kou, B. Vlastakis, A. Petrenko, K. M. Sliwa, A. Narla, S. Shankar, M. J. Hatridge, M. Reagor, L. Frunzio, R. J. Schoelkopf, M. Mirrahimi, and M. H. Devoret, Science **347**, 853 (2015).

[33] S. Touzard, A. Grimm, Z. Leghtas, S. O. Mundhada, P. Reinhold, C. Axline, M. Reagor, K. Chou, J. Blumoff, K. M. Sliwa, S. Shankar, L. Frunzio, R. J. Schoelkopf, M. Mirrahimi, and M. H. Devoret, Phys. Rev. X **8**, 021005 (2018).

[34] R. Lescanne, M. Villiers, T. Peronnin, A. Sarlette, M. Delbecq, B. Huard, T. Kontos, M. Mirrahimi, and Z. Leghtas, Nat. Phys. **16**, 509 (2020).

[35] Z. Wang, C. Navarrete-Benlloch, and Z. Cai, Phys. Rev. Lett. **125**, 115301 (2020).

[36] Y. Chen and C. Navarrete-Benlloch, arXiv:2111.07326.

[37] W.-L. Ma, S. Puri, R. J. Schoelkopf, M. H. Devoret, S. Girvin, and L. Jiang, Sci. Bull. **66**, 1789 (2021).

[38] C. Berdou, A. Murani, U. Réglade, W. C. Smith, M. Villiers, J. Palomo, M. Rosticher, A. Denis, P. Morfin, M. Delbecq, T. Kontos, N. Pankratova, F. Rautschke, T. Peronnin, L.-A. Sellem, P. Rouchon, A. Sarlette, M. Mirrahimi, P. Campagne-Ibarcq, S. Jezouin *et al.*, PRX Quantum **4**, 020350 (2023).

[39] U. Réglade, A. Bocquet, R. Gautier, A. Marquet, E. Albertinale, N. Pankratova, M. Hallén, F. Rautschke, L.-A. Sellem, P. Rouchon, A. Sarlette, M. Mirrahimi, P. Campagne-Ibarcq, R. Lescanne, S. Jezouin, and Z. Leghtas, Nature **629**, 778 (2024).

[40] M. Villiers, W. C. Smith, A. Petrescu, A. Borgognoni, M. Delbecq, A. Sarlette, M. Mirrahimi, P. Campagne-Ibarcq, T. Kontos, and Z. Leghtas, PRX Quantum **5**, 020306 (2024).

[41] *Quantum Squeezing*, edited by P. D. Drummond and Z. Fizek (Springer, Berlin, 2004).

[42] C. Couteau, Contemp. Phys. **59**, 291 (2018).

[43] G. Grynberg, A. Aspect, and C. Fabre, *Introduction to Quantum Optics* (Cambridge University Press, Cambridge, 2010).

[44] C. Navarrete-Benlloch, arXiv:2203.13206.

[45] T. D. Kühner, S. R. White, and H. Monien, Phys. Rev. B **61**, 12474 (2000).

[46] G. G. Batrouni, F. Hébert, and R. T. Scalettar, Phys. Rev. Lett. **97**, 087209 (2006).

[47] D. Rossini and R. Fazio, New J. Phys. **14**, 065012 (2012).

[48] G. G. Batrouni, R. T. Scalettar, V. G. Rousseau, and B. Grémaud, Phys. Rev. Lett. **110**, 265303 (2013).

[49] K. Kawaki, Y. Kuno, and I. Ichinose, Phys. Rev. B **95**, 195101 (2017).

[50] K. Yamamoto, S. Todo, and S. Miyashita, Phys. Rev. B **79**, 094503 (2009).

[51] K. Suthar, H. Sable, R. Bai, S. Bandyopadhyay, S. Pal, and D. Angom, Phys. Rev. A **102**, 013320 (2020).

[52] U. Schollwöck, Ann. Phys. (NY) **326**, 96 (2011).

[53] A. E. Feiguin, AIP Conf. Proc. **1419**, 5 (2011).

[54] B. Schmidt, Exact numerical simulations of strongly interacting atoms in 1D trap potentials and optical lattices, Ph.D. thesis, Technischen Universität Kaiserslautern, 2009.

[55] Y. Tomita and Y. Okabe, Phys. Rev. B **66**, 180401(R) (2002).

[56] K. Binder, Z. Phys. B **43**, 119 (1981).

[57] M. Iskin and J. K. Freericks, Phys. Rev. A **79**, 053634 (2009).

[58] M. Iskin, Phys. Rev. A **83**, 051606(R) (2011).

[59] S. Sachdev, *Quantum Phase Transitions* (Cambridge University Press, Cambridge, 2011).

[60] N. Carlon Zambon, S. R. K. Rodriguez, A. Lemaître, A. Harouri, I. Le Gratiet, I. Sagnes, P. St-Jean, S. Ravets, A. Amo, and J. Bloch, Phys. Rev. A **102**, 023526 (2020).

[61] C. K. Law, H. Pu, and N. P. Bigelow, Phys. Rev. Lett. **81**, 5257 (1998).

[62] S. Yi, O. E. Müstecaplıoğlu, C. P. Sun, and L. You, Phys. Rev. A **66**, 011601(R) (2002).

[63] T.-C. Guo and L. You, Front. Phys. **10**, 847409 (2022).

[64] E. Timmermans, P. Tommasini, R. Côté, M. Hussein, and A. Kerman, Phys. Rev. Lett. **83**, 2691 (1999).

[65] J. Javanainen and M. Mackie, Phys. Rev. A **59**, R3186 (1999).

[66] D. J. Heinzen, R. Wynar, P. D. Drummond, and K. V. Kheruntsyan, Phys. Rev. Lett. **84**, 5029 (2000).

[67] O. Jamadi, B. Real, K. Sawicki, C. Hainaut, A. González-Tudela, N. Pernet, I. Sagnes, M. Morassi, A. Lemaitre, L. L. Gratiet, A. Harouri, S. Ravets, J. Bloch, and A. Amo, arXiv:2112.07753.

[68] C. W. Gardiner and Zoller, *Quantum Noise* (Springer, New York, 2004).

[69] H. J. Carmichael, *Statistical Methods in Quantum Optics 1* (Springer, Berlin, 2002).

[70] H.-P. Breuer and F. Petruccione, *The Theory of Open Quantum Systems* (Oxford University Press, Oxford, 2002).

[71] *Nonclassical Effects in Quantum Optics*, edited by P. Meystre and D. Walls (American Institute of Physics, New York, 1991).

[72] P. Deuar, A. Ferrier, M. Matuszewski, G. Orso, and M. H. Szymańska, PRX Quantum **2**, 010319 (2021).

[73] P. Deuar, Quantum **5**, 455 (2021).

[74] J. A. Ross, P. Deuar, D. K. Shin, K. F. Thomas, B. M. Henson, S. S. Hodgman, and A. G. Truscott, Sci. Rep. **12**, 13178 (2022).

[75] L. M. Sieberer, M. Buchhold, and S. Diehl, Rep. Prog. Phys. **79**, 096001 (2016).

[76] H. Weimer, A. Kshetrimayum, and R. Orús, Rev. Mod. Phys. **93**, 015008 (2021).

[77] P. Werner, K. Völker, M. Troyer, and S. Chakravarty, Phys. Rev. Lett. **94**, 047201 (2005).

[78] L. Capriotti, A. Cuccoli, A. Fubini, V. Tognetti, and R. Vaia, Phys. Rev. Lett. **94**, 157001 (2005).

[79] S. Morrison and A. S. Parkins, J. Phys. B **41**, 195502 (2008).

[80] J. Eisert and T. Prosen, arXiv:1012.5013.

[81] E. M. Kessler, G. Giedke, A. Imamoglu, S. F. Yelin, M. D. Lukin, and J. I. Cirac, Phys. Rev. A **86**, 012116 (2012).

[82] B. Horstmann, J. I. Cirac, and G. Giedke, Phys. Rev. A **87**, 012108 (2013).

[83] D. J. Griffiths and D. F. Schroeter, *Introduction to Quantum Mechanics* (Cambridge University Press, Cambridge, 2017).

[84] C. Navarrete-Benlloch, *An Introduction to the Formalism of Quantum Information with Continuous Variables* (Morgan & Claypool, San Rafael, 2015).

[85] C. Weedbrook, S. Pirandola, R. García-Patrón, N. J. Cerf, T. C. Ralph, J. H. Shapiro, and S. Lloyd, Rev. Mod. Phys. **84**, 621 (2012).

[86] S. L. Braunstein and P. van Loock, Rev. Mod. Phys. **77**, 513 (2005).

[87] A. Ferraro, S. Olivares, and M. G. A. Paris, *Gaussian States in Quantum Information* (Bibliopolis, Naples, 2005).

[88] L. Mandel and E. Wolf, *Optical Coherence and Quantum Optics* (Cambridge University Press, Cambridge, 1995).

[89] T. Shi, E. Demler, and J. I. Cirac, Ann. Phys. (NY) **390**, 245 (2018).

[90] P. Kinsler and P. D. Drummond, Phys. Rev. A **43**, 6194 (1991).

[91] C. Navarrete-Benlloch, G. Patera, and G. J. de Valcárcel, Phys. Rev. A **96**, 043801 (2017).

[92] I. de Vega, D. Porras, and J. I. Cirac, Phys. Rev. Lett. **101**, 260404 (2008).

[93] C. Navarrete-Benlloch, I. de Vega, D. Porras, and J. I. Cirac, New J. Phys. **13**, 023024 (2011).

[94] H. J. Carmichael, *Statistical Methods in Quantum Optics 2* (Springer, Berlin, 2008).